3 RESULTS AND DISCUSSION

3.1 Synthesis of ligand

The 2-(phenylazo)benzothiazole or bsazpy ligand was synthesized by condensing nitrosobenzene with 2-aminobenzothiazole in the mixture of NaOH and benzene. The product was chromatographically separated as red-orange band (34%yield). The reaction is shown in equation (1).

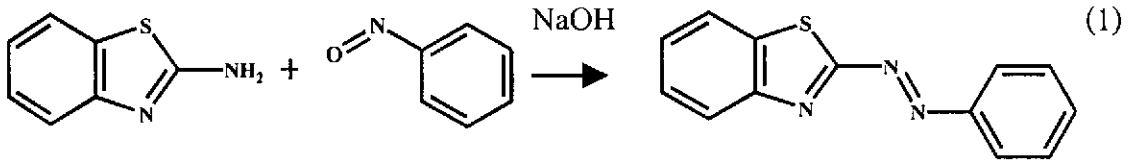

(1)

2-aminobenzothiazole nitrosobenzene 2-(phenylazo)benzothiazole (bsazpy)

The physical properties of the bsazpy ligand are shown in Table 1.

Table 1. The physical properties of the bsazpy ligand

Ligand	Physical properties		
	Appearance	Color	Melting point (°C)
bsazpy	Solid	Red-orange	143-145

The 2-(phenylazo)benzothiazole or bsazpy ligand is a new ligand containing azoimine functional group, -N=N-C=N-, which is π-acidic and stabilizes low valence metals such as Cu(I), Ru(II). The bsazpy acts as a *N,N'*-chelating molecules. The donor

centers are abbreviated as N(benzothiazole), N and N(azo), N′. The atom numbering scheme is shown in the Figure 2.

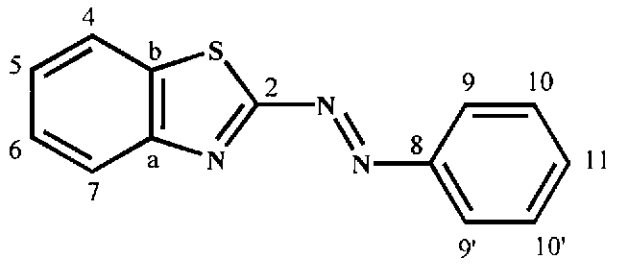

Figure 2. The structure of the bsazpy ligand.

3.2 Characterization of ligand

The chemistry of ligand was investigated by using the following techniques :

3.2.1 Elemental Analysis

3.2.2 Fast-atom bombardment Mass Spectrometry (FAB-MS)

3.2.3 UV-Visible Absorption Spectroscopy (UV-Vis)

3.2.4 Infrared Spectroscopy (IR)

3.2.5 Nuclear Magnetic Resonance Spectroscopy (NMR; 1D and 2D)

3.2.6 Cyclic Voltammetry (CV)

3.2.1 Elemental Analysis

Elemental Analysis is a principle method used to study composition of elements in compound. The elemental analysis data are shown in Table 2.

Table 2. Elemental analysis data of the bsazpy ligand

Ligand	% C		% H		% N	
	Calc.	Found	Calc.	Found	Calc.	Found
bsazpy	65.25	65.37	3.79	3.92	17.56	17.46

From the elemental analysis data, the analytical values corresponded to the calculated values. Therefore, the composition of elements in bsazpy ligand was confirmed by this method.

3.2.1 Fast-Atom Bombardment (FAB) Mass Spectrometry

The FAB mass spectrometry is a basic technique used to determine molecular mass of compound. The FAB mass spectroscopic data are shown in Table 3 and the FAB mass spectrum of the bsazpy ligand is shown in Figure 3.

Table 3. FAB mass spectroscopic data of the bsazpy ligand

m/z	Stoichiometry	Equivalent species	Rel. Abun. (%)
240	$[bsazpy + H]^+$	$[M + H]^+$	100
105	$[C_6H_5N_2]^+$	-	30

M = Molecular weight of bsazpy = 239.23 g/mol

From the FAB mass spectroscopic data, the maximum peak which gave 100% relative abundance at m/z 240 corresponded to the molecular weight of bsazpy with one protonation. Thus, the expected molecular weight was supported by this method.

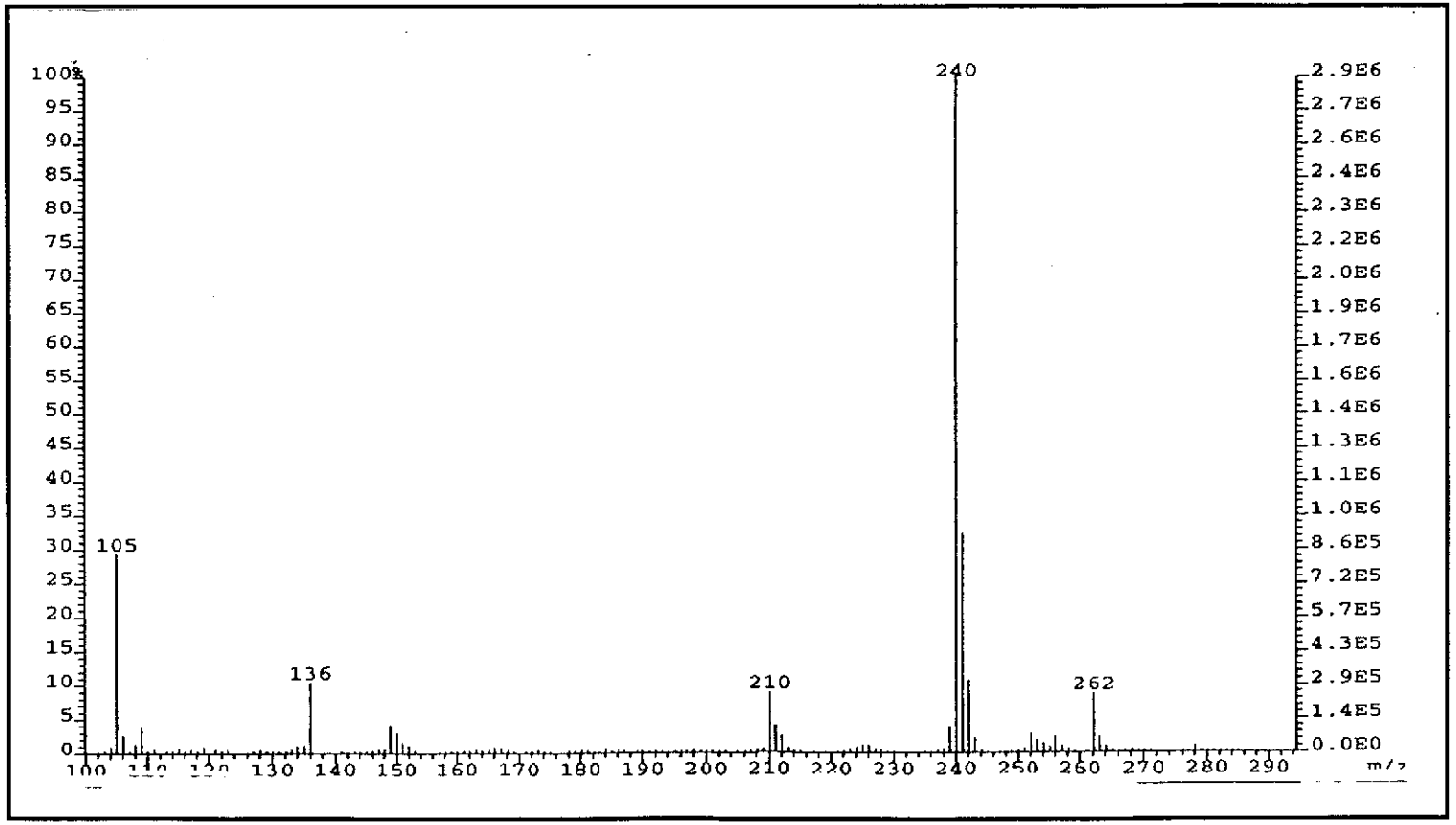

Figure 3. FAB mass spectrum of the bsazpy ligand.

3.2.2 UV-Visible Absorption Spectroscopy

UV-Visible absorption spectroscopy is a technique used to study the electronic transition of compound. The UV-Visible absorption spectra of the bsazpy ligand in various solvents; CH_2Cl_2, $CHCl_3$, CH_3CN, DMF and DMSO were recorded in the range 200-800 nm. The UV-Visible spectroscopic data of bsazpy are collected in Table 4 and the absorption spectrum of bsazpy in CH_2Cl_2 is shown in Figure 4.

Table 4. The electronic spectral data of the bsazpy ligand

Solvents	λ_{max}, nm (10^{-4} ε^a, $M^{-1}cm^{-1}$)
CH_2Cl_2	369 (2.09)
$CHCl_3$	370 (2.09)
CH_3CN	366 (2.08)
DMF	371 (1.98)
DMSO	374 (1.74)

[a] Molar extinction coefficient

The electronic spectra of bsazpy in various solvents displayed absorption in the range 200-600 nm. The bsazpy exhibited intense absorption band at around 365-375 nm ($\varepsilon \sim 20000\ M^{-1}cm^{-1}$) which was assigned to $\pi \longrightarrow \pi^*$ transition and the very low intensity band in visible region was assigned to $n \longrightarrow \pi^*$ transition. The very low intensity of $n \longrightarrow \pi^*$ absorption band may be due to the more π-conjugation character in benzothiazole ring. Similarly, the azpy ligand exhibited two absorption bands in UV and visible regions which were assigned to $\pi \longrightarrow \pi^*$ and $n \longrightarrow \pi^*$ transitions, respectively.

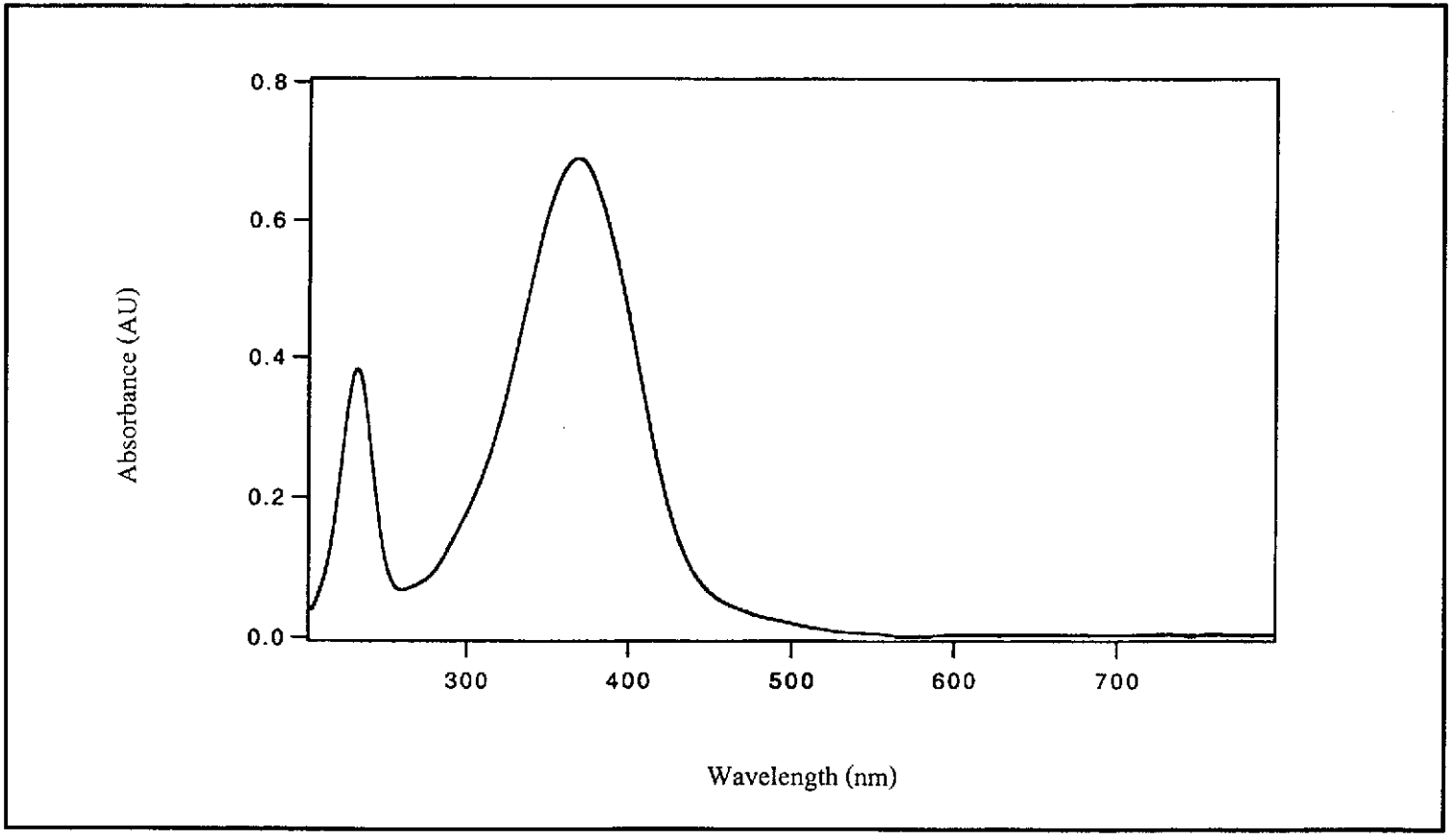

Figure 4. UV-Visible absorption spectrum of bsazpy in CH_2Cl_2.

3.2.3 Infrared Spectroscopy

Infrared spectroscopy is an useful technique used to study the important functional groups in molecule. Infrared spectrum of bsazpy was recorded in the range 4000-400 cm^{-1} and shown in Figure 5. The selected spectral data are collected in Table 5.

Table 5. The selected infrared spectroscopic data of the bsazpy ligand

Vibration modes	Frequencies (cm^{-1})
C=N, C=C stretching	1491 (m) 1458 (s)
N=N stretching	1317 (s)
C-H bending of monosubstituted benzene	757 (s) 728 (s) 680 (s)

s = strong, m = medium

From the infrared spectrum of bsazpy, the intense peaks in the range 1600-600 cm^{-1}, which were characteristic of aromatic system, were observed. There were several stretching modes which belonged to benzothiazole ring, phenyl ring such as C=C, C=N stretching modes and C-H bending modes of monosubstituted benzene.

The most important peak was the N=N stretching mode which was used to consider the π-acid property in azo compounds. The presence of a strong N=N stretching at 1317 cm^{-1} in bsazpy indicated the presence of an azoimine chromophore in the molecule and it appeared at lower frequency than that of azpy, 1424 cm^{-1} (Krause

and Krause, 1980). The results indicated that the N=N bond of free azpy ligand is stronger than that of bsazpy ligand.

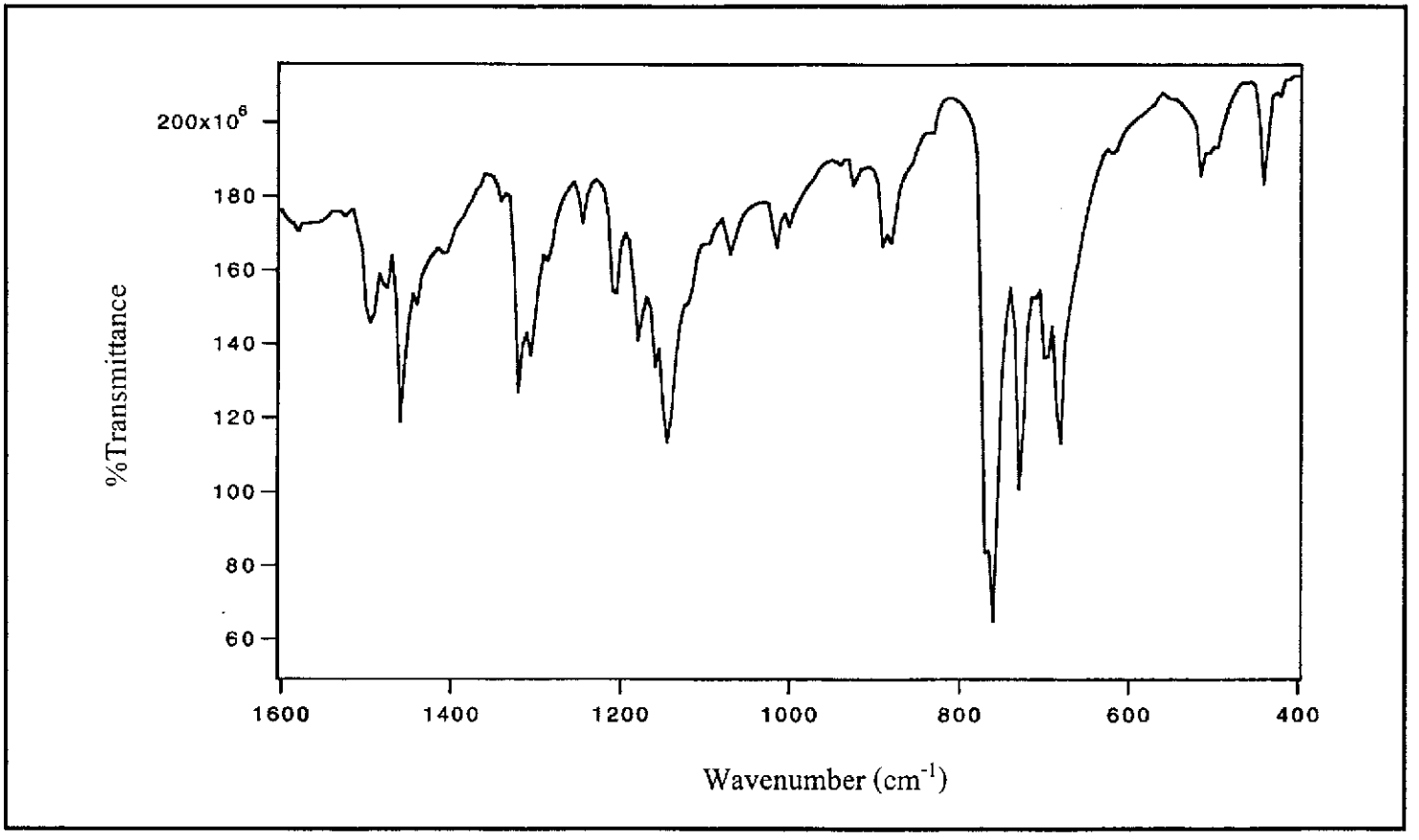

Figure 5. IR spectrum of the bsazpy ligand.

3.2.4 Nuclear Magnetic Resonance Spectroscopy

Nuclear Magnetic Resonance spectroscopy is an important technique for determining molecular structure of compound. The structure of bsazpy ligand was determined by using 1D and 2D NMR spectroscopic techniques; ^{1}H NMR, ^{1}H-^{1}H COSY NMR, ^{13}C NMR, DEPT NMR, ^{1}H-^{13}C NMR. The NMR spectra of bsazpy were recorded in $CDCl_3$ on UNITY SNOVA 500 MHz. The tetramethylsilane (TMS, $(CH_3)_4Si$) was used as an internal reference. The atom numbering scheme of the bsazpy ligand is shown in Figure 6.

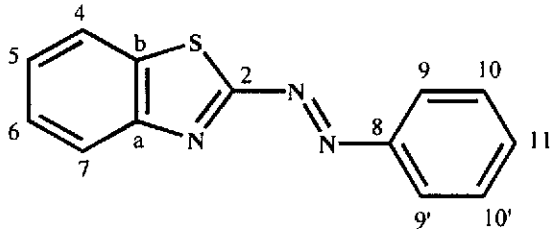

Figure 6. The atom numbering scheme of bsazpy.

The chemical shift and *J*-coupling constant data of bsazpy ligand are listed in Table 6 and NMR spectra are shown in Figure 7 to Figure 11.

Table 6. ^{1}H NMR and ^{13}C NMR spectroscopic data of the bsazpy ligand

Positions	^{1}H NMR			^{13}C NMR
	δ(ppm)	J (Hz)	Number of H	δ(ppm)
7	8.19 (dd)	8.17, 1.22	1	125.01
9	8.07 (m)	-	2	124.29
4	7.89 (dd)	7.99, 1.28	1	122.32
10	7.58 (m)	-	2	129.42
11	7.58 (m)	-	1	133.58
6	7.53 (td)	7.61, 1.34	1	126.70
5	7.47 (td)	7.70, 1.22	1	127.54
2	-	-	-	175.64
a	-	-	-	152.07
b	-	-	-	151.64
8	-	-	-	134.44

dd = doublet of doublet, td = triplet of doublet, m = multiplet

The ^{1}H NMR spectrum of bsazpy ligand (Figure 7) displayed 7 resonance signals for 9 protons which belonged to the benzothiazole ring and the phenyl ring. The detail of each signal could be explained below.

The proton H4 resonance appeared at 7.89 ppm as doublet of doublet (dd) due to the coupling with proton H5 (J = 7.99 Hz) and proton H6 (J = 1.28 Hz).

The proton H5 located between proton H4 and proton H6 on the benzothiazole

ring. This signal appeared as triplet of doublet (td) at 7.47 ppm. The splitting of triplet peaks were observed for the vicinal coupling (J = 7.70 Hz). The long range coupling with proton H7 gave the doublet peaks (J = 1.22 Hz).

The proton H6 showed the triplet of doublet (td) peaks at 7.53 ppm. The splitting of triplet peaks were observed for the vicinal coupling (J = 7.61 Hz). The doublet peaks were occurred due to the long range coupling with proton H4 (J = 1.34 Hz).

The proton H7 located close to the benzothiazole nitrogen atom, occurred at most downfield. The resonance occurred as doublet of doublet (dd) at 8.19 ppm. The splitting of doublet of doublet peaks were observed for coupling with proton H6 (J = 8.17 Hz) and proton H5 (J = 1.22 Hz).

The proton H9 were two equivalent protons on the phenyl ring located close to the azo nitrogen. The signal showed multiplet (m) peaks at 8.07 ppm.

The proton H10 were two equivalent protons located next to proton H9. The resonance showed multiplet (m) peaks at 7.58 ppm.

The proton H11 located next to proton H10. The splitting pattern was multiplet (m) at the same position of proton H10 (7.58 ppm).

In addition, the peak assignment was studied by using COSY NMR spectrum (Figure 8), which showed the correlation of ^{1}H-^{1}H coupling.

The results from ^{13}C NMR spectrum (Figure 9) corresponded to the results of DEPT NMR spectrum (Figure 10), which showed only methine carbon signals. The ^{13}C NMR spectrum of bsazpy ligand showed 11 signals for 13 carbon. The quaternary carbon C2 signal on benzothiazole ring appeared at the most downfield (175.64 ppm). The signals at 152.07 and 151.64 ppm belonged to quaternary carbon Ca and quaternary carbon Cb, respectively. The signal of quaternary carbon C8 on the phenyl ring occurred at 134.44 ppm. The carbon C11 signal on phenyl ring occurred at 133.58 ppm. The signals at 129.42 and 124.29 ppm were assigned to two equivalent carbon of carbon C10

and carbon C9. The signals of carbon C5, carbon C6, carbon C7 and carbon C4 of benzothiazole ring were observed at 127.54, 126.70, 125.01 and 122.32 ppm, respectively.

Moreover, the ^{13}C NMR signals assignments were supported by the HMQC NMR spectrum (Figure 11), which showed the correlation between ^{1}H NMR and ^{13}C NMR spectra.

The results from NMR data together with the expected structure, thus confirmed the molecular structure of the bsazpy ligand.

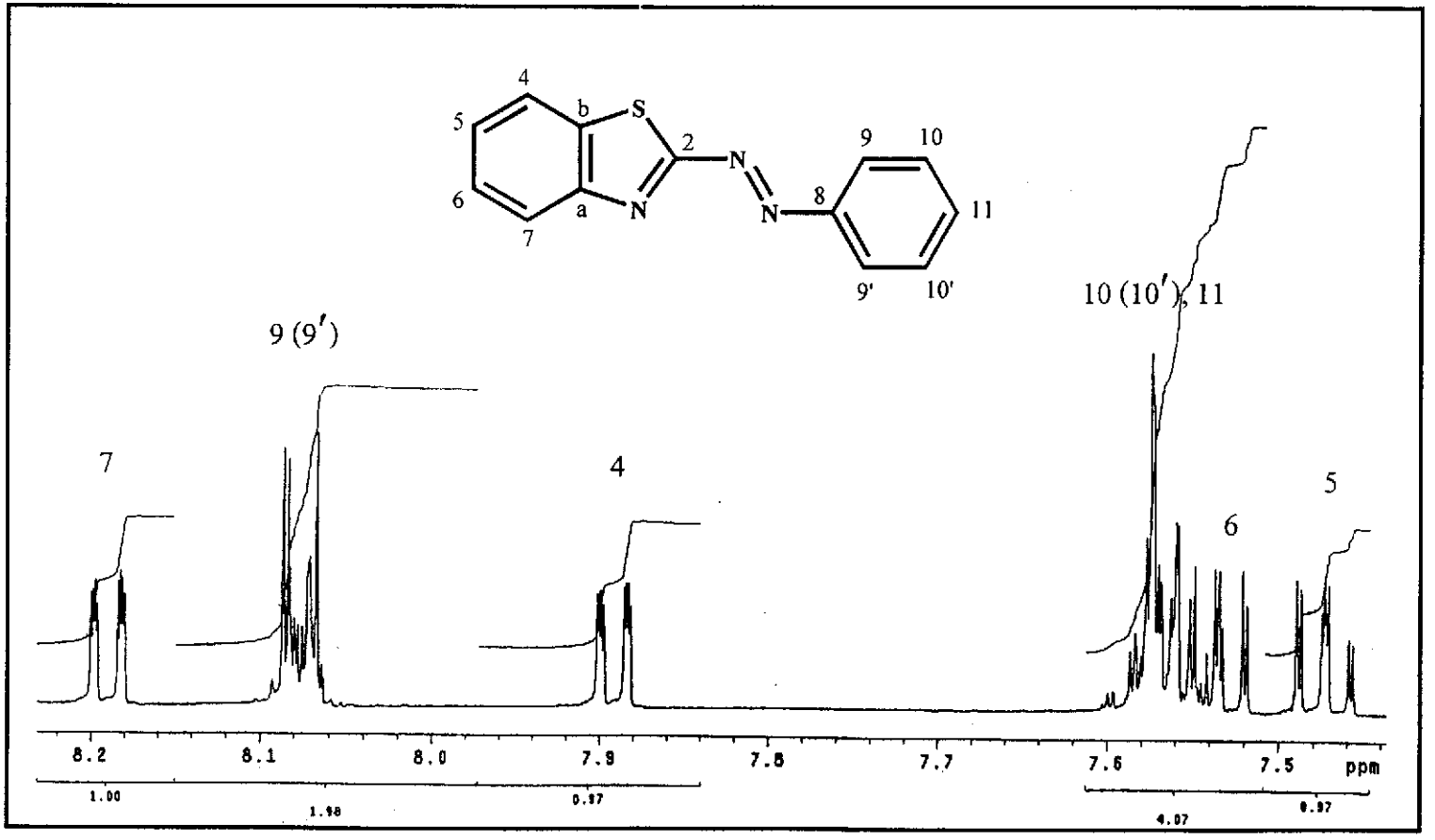

Figure 7. ^{1}H NMR spectrum of bsazpy in $CDCl_3$ (500 MHz).

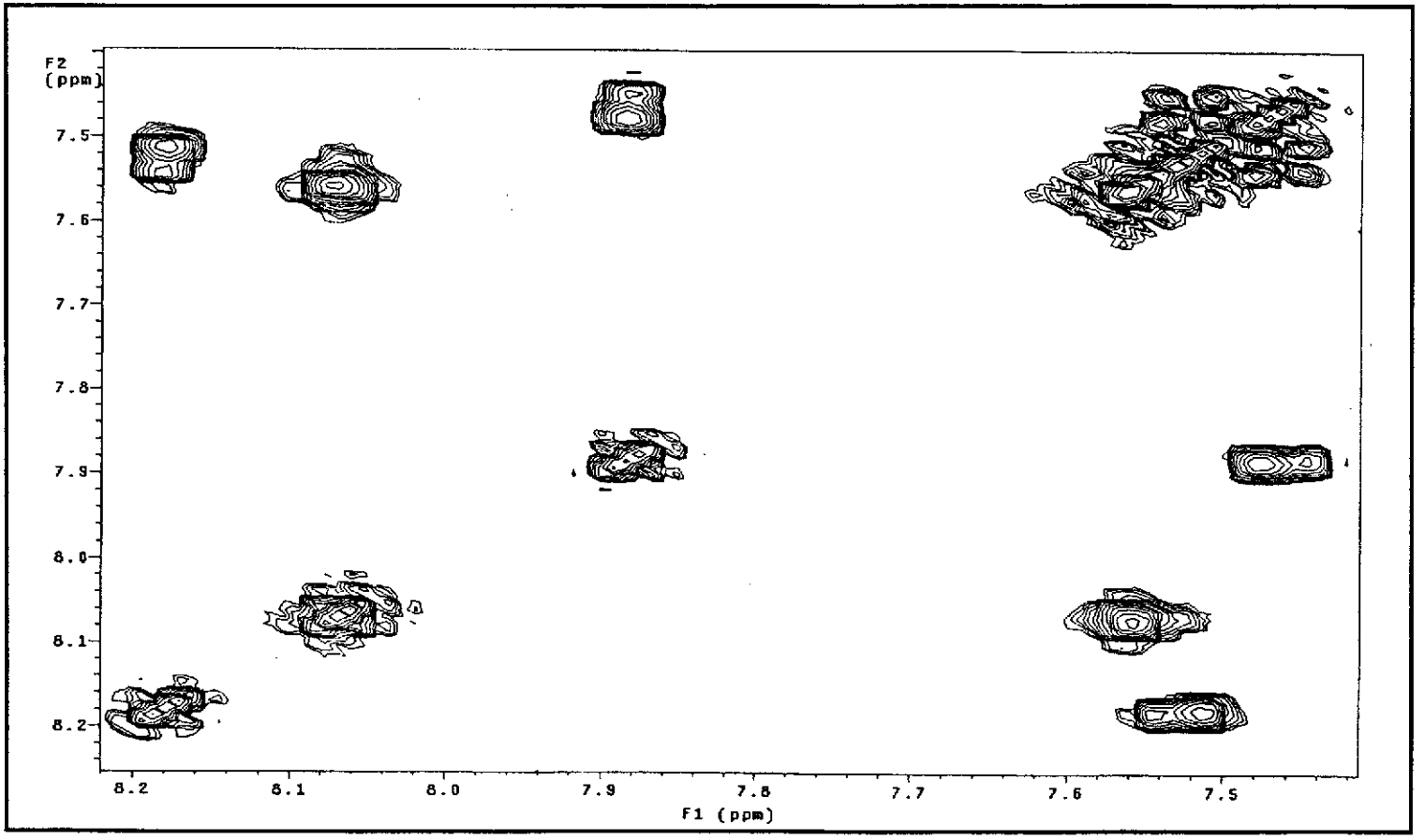

Figure 8. ^{1}H-^{1}H COSY NMR spectrum of bsazpy in $CDCl_3$ (500 MHz).

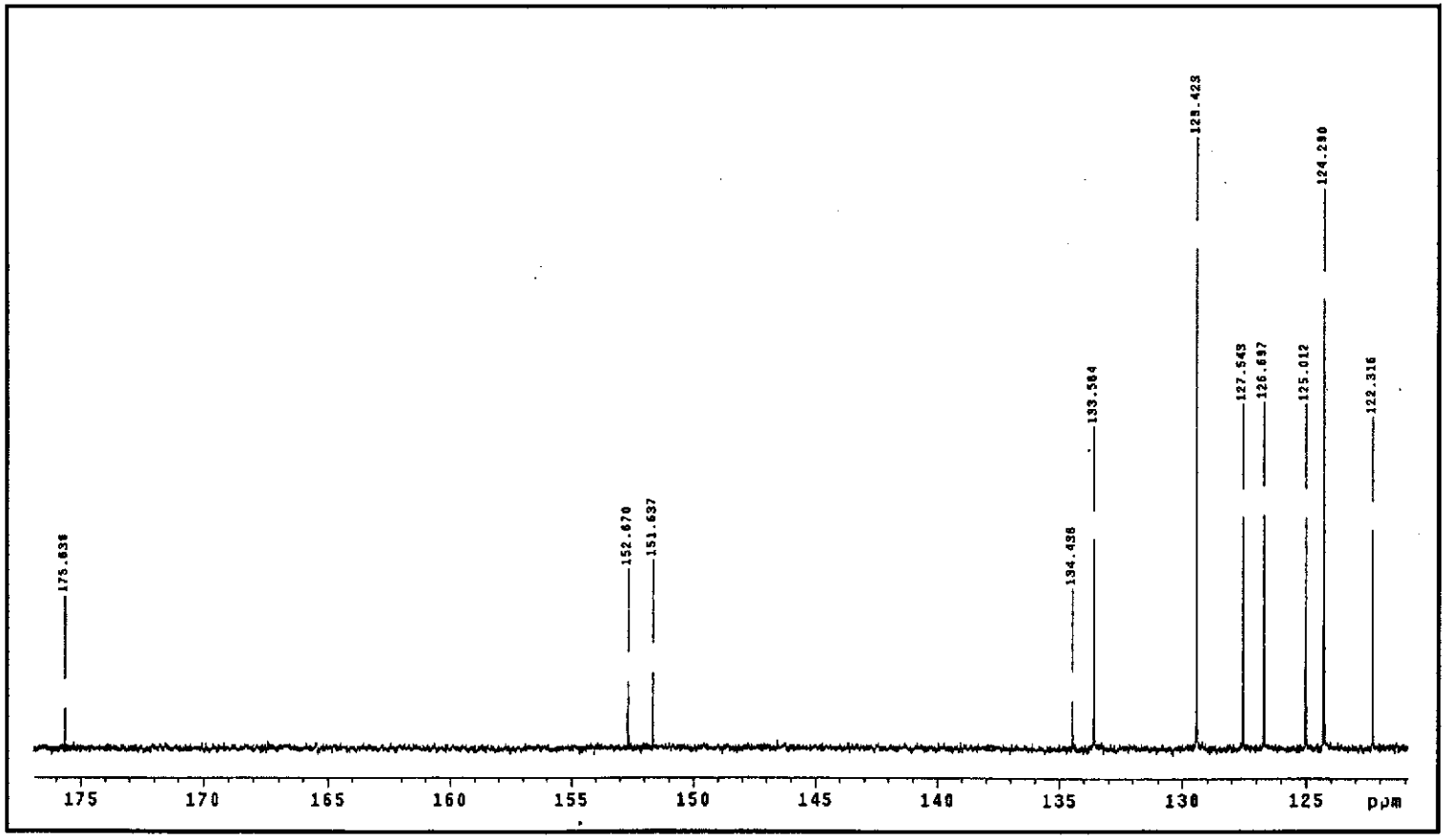

Figure 9. ^{13}C NMR spectrum of bsazpy in $CDCl_3$ (500 MHz).

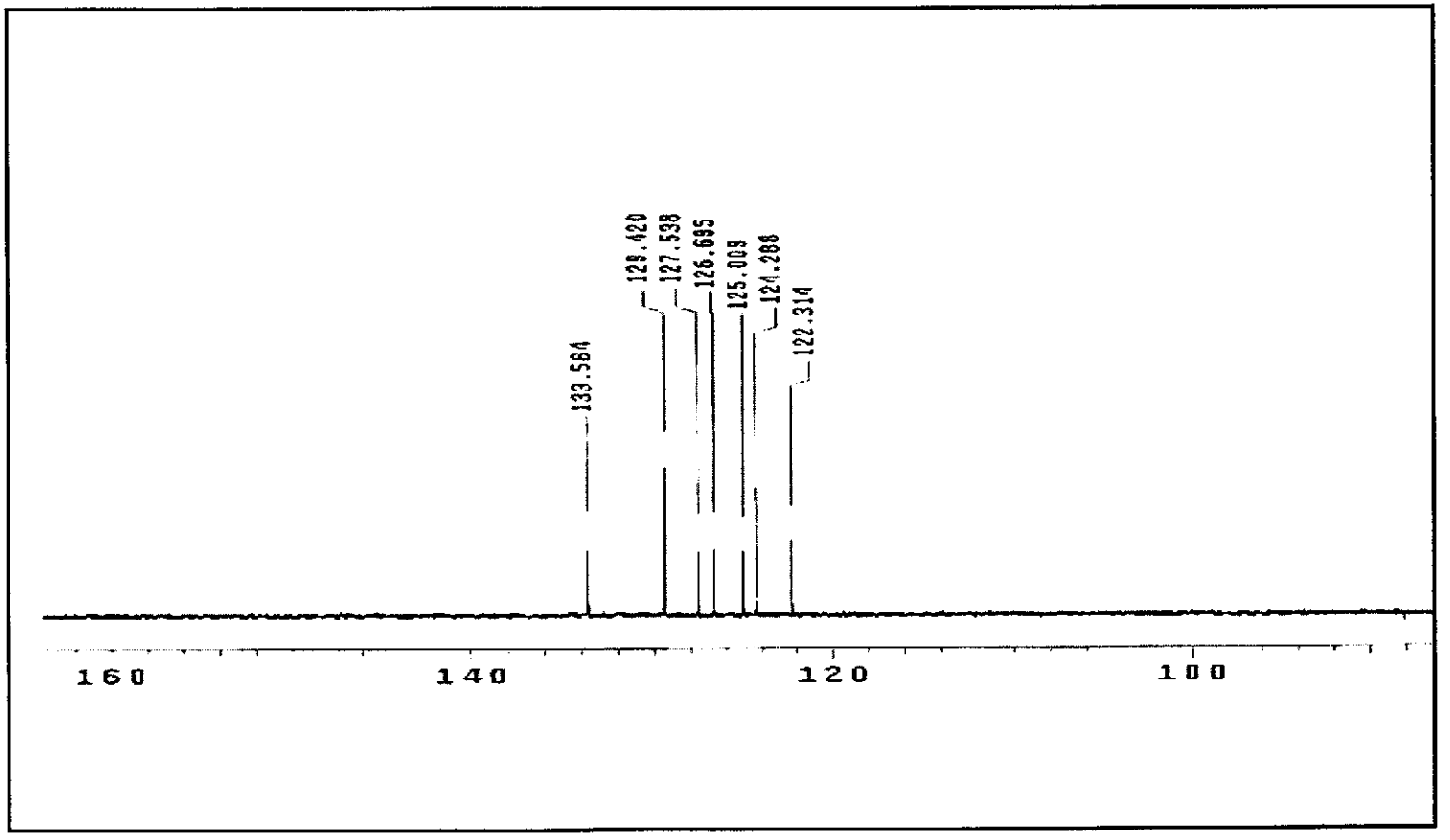

Figure 10. DEPT NMR spectrum of bsazpy in $CDCl_3$ (500 MHz).

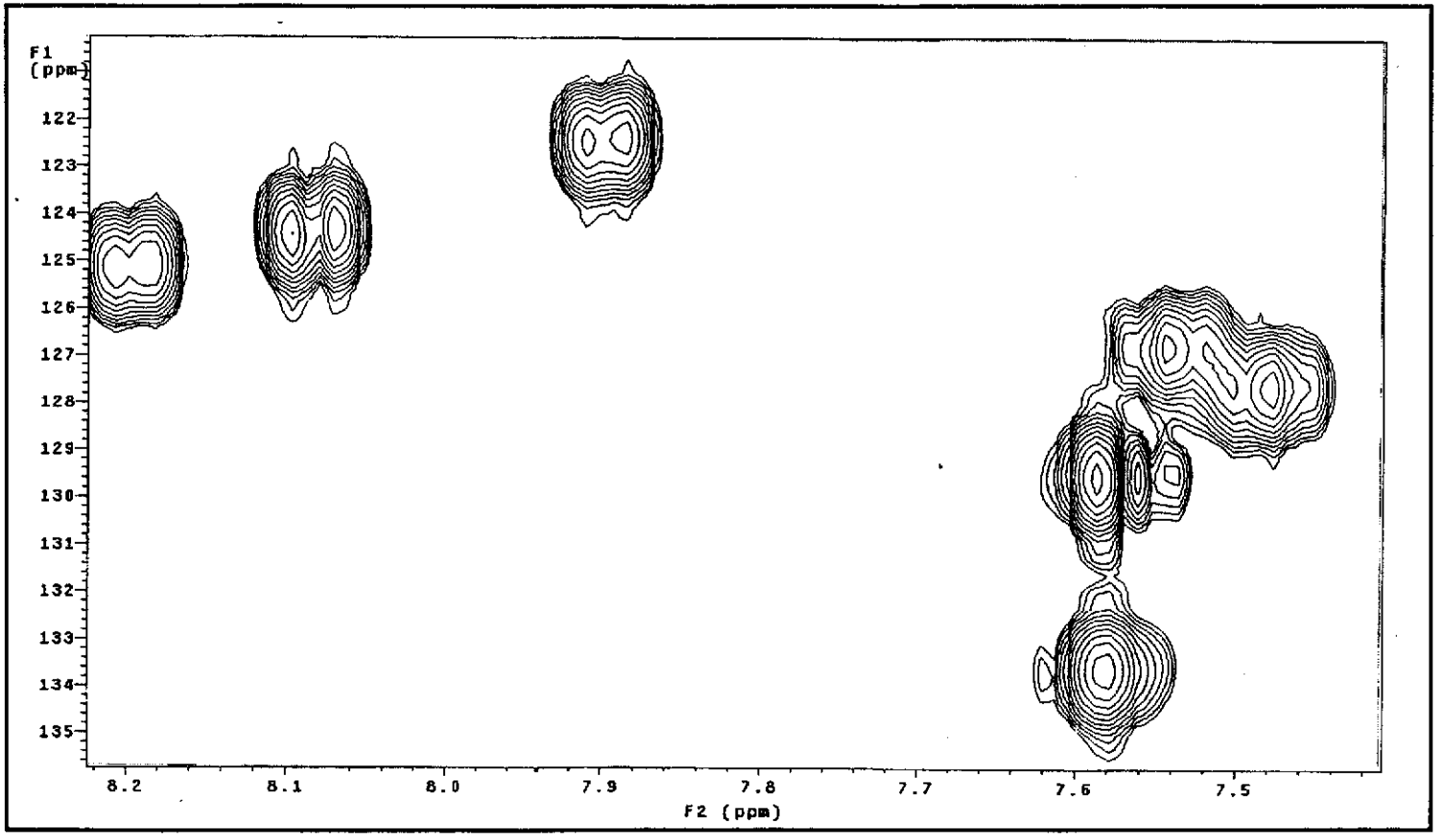

Figure 11. ^{1}H-^{13}C HMQC NMR spectrum of bsazpy in $CDCl_3$ (500 MHz).

3.2.5 Cyclic Voltammetry

Cyclic voltammetry is an electrochemical technique used to study the redox behavior of ligand. The potentials were reported with reference to the ferrocene couple. The cyclic voltammograms in dichloromethane solution of the bsazpy and the azpy ligands are shown in Figure 12 and Figure 13, respectively. The cyclic voltammetric data of both ligands are listed in Table 7.

In this work, the different scan rates were used to check the couple or the redox reaction. The couple giving equal anodic and cathodic currents was referred to reversible couple. On the other hand, the unequal currents were referred to the unequally transfer of the electron in the reduction and oxidation which led to irreversible couple.

Table 7. Cyclic voltammetric data of bsazpy and azpy in 0.1 M TBAH dichloromethane at scan rate 50 mV/s (ferrocene as internal standard, ΔE_p = 130 mV)

Ligands	$E_{1/2}$, V (ΔE_p, mV)	
	Oxidation	Reduction
bsazpy	-	-1.27 (135)
azpy	-	-1.96[a]

[a] Cathodic peak (Ep_c)

Reduction range

The ligands reduction were studied in the range 0.00 to –2.00 V. The bsazpy ligand showed one quasi-reversible couple with two electron transfer process at –1.27 V with peak-to-peak separation 135 mV, corresponding to the electron acceptance of the azo function as Eq.(2).

$$\text{bsazpy} + 2e^- \rightleftharpoons \text{bsazpy}^{2-} \quad \ldots. (2)$$

The free azpy ligand displayed one irreversible couple in reduction range. It indicated that azpy ligand accepted two electrons in its lowest unoccupied molecular orbital (LUMO) which was primary azo in character (Goswami, et al., 1983) as Eq.(3).

$$\text{azpy} + 2e^- \rightleftharpoons \text{azpy}^{2-} \quad \ldots. (3)$$

The electron accepting ability of ligand was considered in the reduction range. The more positive potential was the greater electron accepting ability. Comparison with azpy, the bsazpy ligand showed ligand reduction (-1.27 V) at higher potential than that of azpy (-1.96 V). Thus, it may be conclude that the bsazpy ligand can accept electron better than the azpy ligand. This result corresponded to the infrared spectroscopic data shown by the N=N stretching at lower frequency of the former ligand.

Oxidation range

The cyclic voltammograms of the bsazpy and the azpy ligands showed no signal in the potential range 0.00 to +1.50 V.

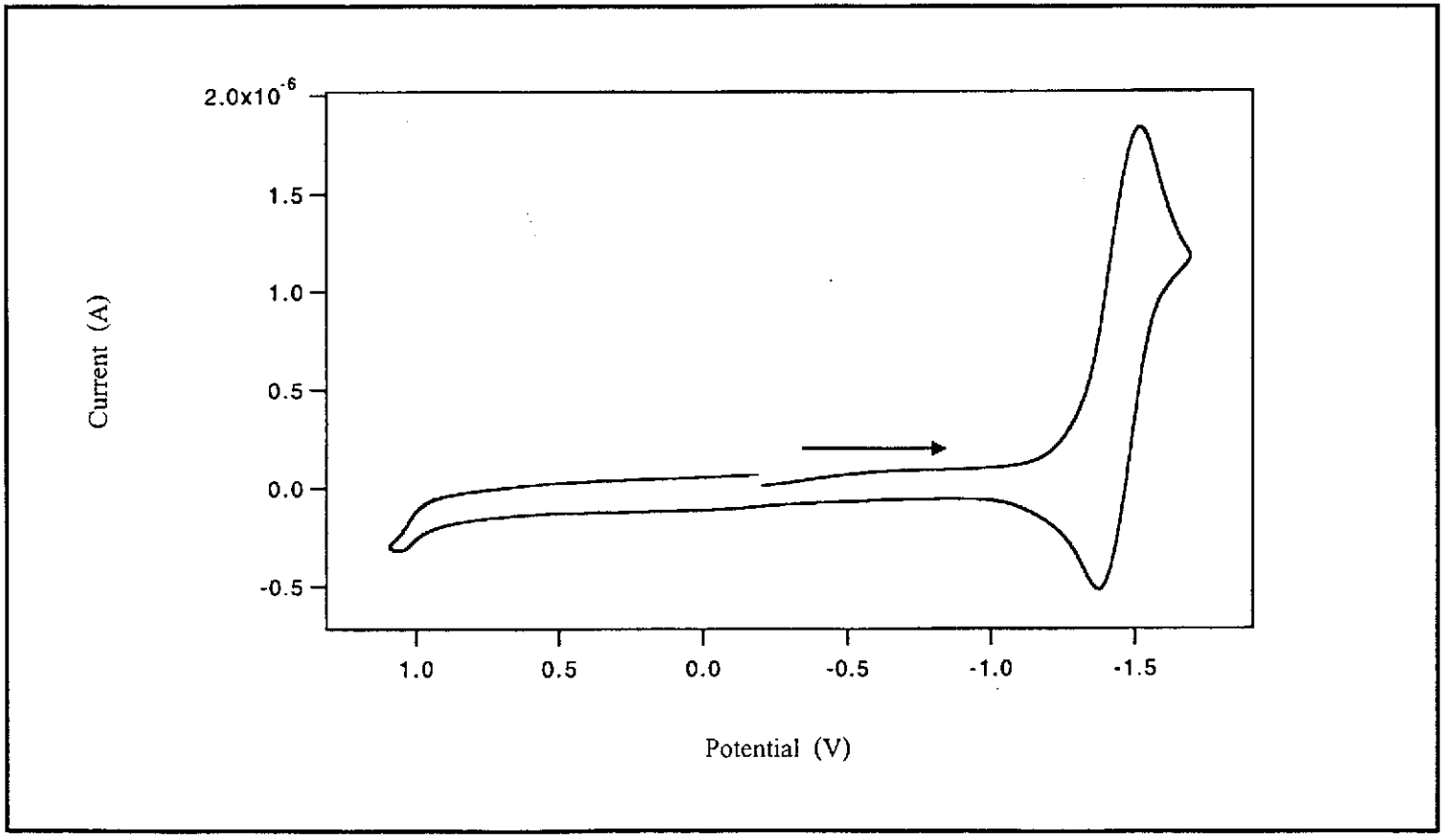

Figure 12. Cyclic voltammogram of bsazpy in 0.1 M TBAH CH_2Cl_2 at scan rate 50 mV/s.

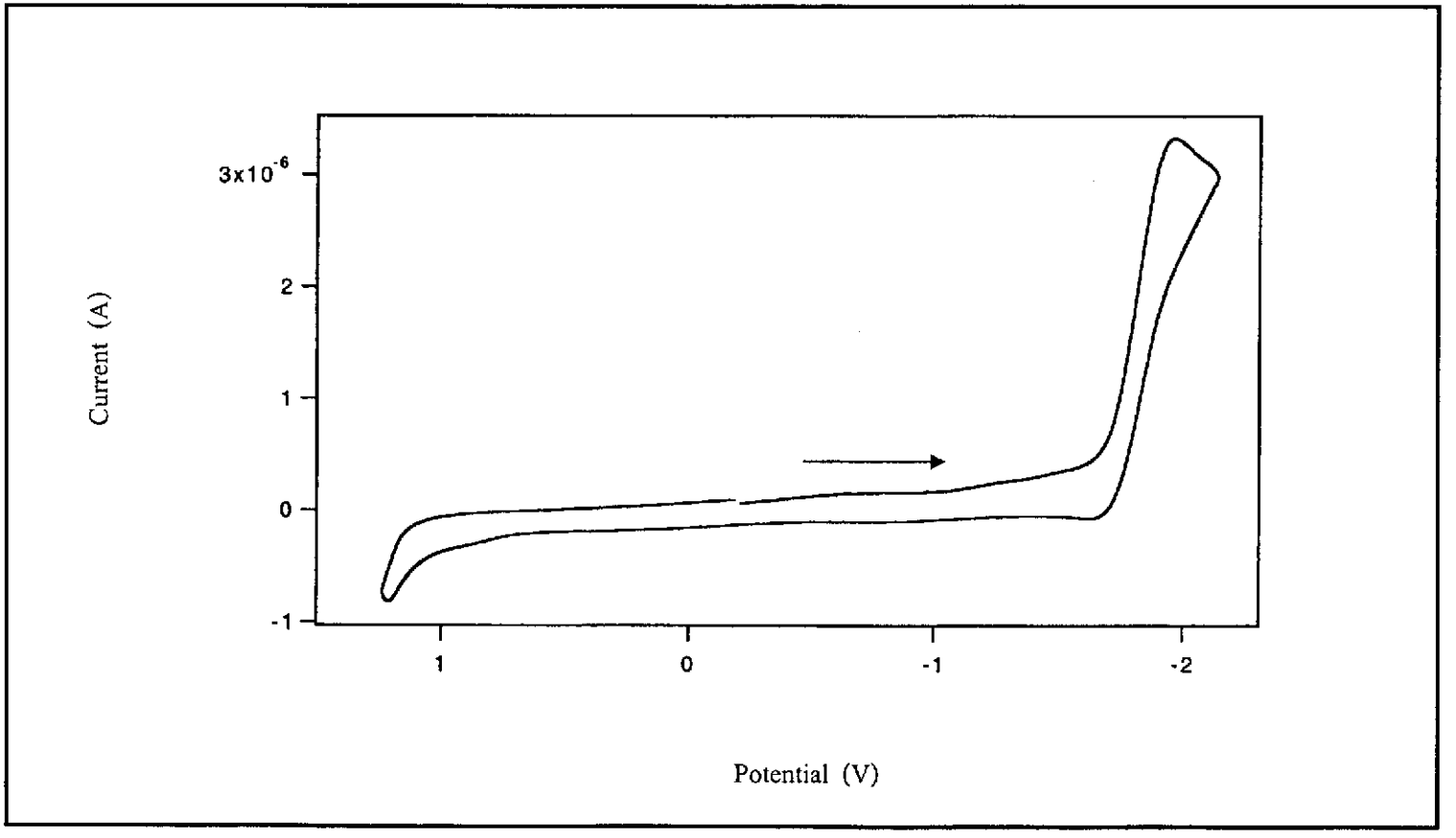

Figure 13. Cyclic voltammogram of azpy in 0.1 M TBAH CH_2Cl_2 at scan rate 50 mV/s.

3.3 Synthesis of complexes

Hydrated ruthenium(III) chloride reacted with the 2-(phenylazo)benzothiazole (bsazpy) in ethanol to yield the isomeric $Ru(bsazpy)_2Cl_2$ complexes (Eq. (4)). Purification was carried out by column chromatography. The three geometrical isomers were isolated as *ctc*-, *cct*- and *ttt*- isomers.

$$bsazpy + RuCl_3.3H_2O \rightarrow [Ru(bsazpy)_2Cl_2] \quad \ldots\ldots (4)$$

The physical properties of the $[Ru(bsazpy)_2Cl_2]$ complexes are listed in Table 8.

Table 8. The physical properties of the $[Ru(bsazpy)_2Cl_2]$ complexes

Complexes	Physical properties		
	Appearance	Color	Melting point (°C)
ctc-$[Ru(bsazpy)_2Cl_2]$	Solid	Purple	347-348
cct-$[Ru(bsazpy)_2Cl_2]$	Solid	Green	345-346
ttt-$[Ru(bsazpy)_2Cl_2]$	Solid	Dark-Green	346-347

The bsazpy is an unsymmetrical N,N'- bidentate ligand and lacks a twofold symmetry axis. Theoretically, the pseudo-octahedral dichloro species, $[Ru(bsazpy)_2Cl_2]$ can occur in five geometrical isomeric forms: *trans-cis-cis* [*tcc*, (I)], *trans-trans-trans* [*ttt*, (II)], *cis-trans-cis* [*ctc*, (III)], *cis-cis-trans* [*cct*, (IV)] and *cis-cis-cis* [*ccc*, (V)] with coordinating pairs in the order Cl, N_b (N(benzothiazole)) and N_a (N(azo)) as Figure 14. In the present work three isomers were isolated and spectroscopically characterized as

cis-trans-cis (*ctc*) , *cis-cis-trans* (*cct*) and *trans-trans-trans* (*ttt*) complexes. The structures of *ctc*- and *cct*- isomers were confirmed by X-ray diffraction studies.

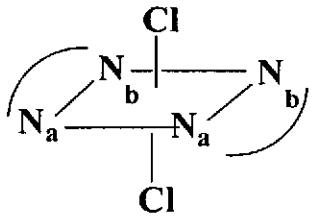

tcc (I)

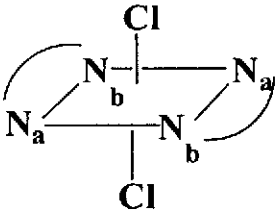

ttt (II)

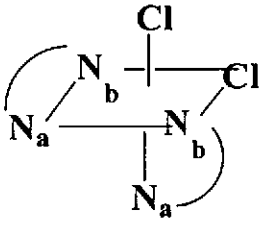

ctc (III)

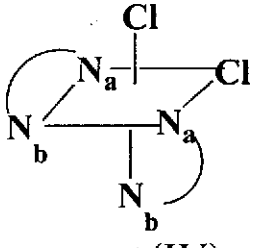

cct (IV)

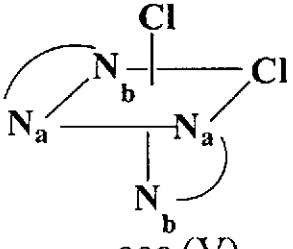

ccc (V)

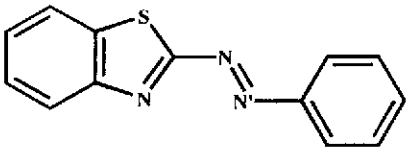

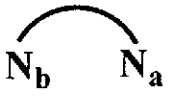

N_b : N(benzothiazole)

N_a : N(azo)

Figure 14. Five possible isomers of the $[RuL_2Cl_2]$ complexes.

3.4 Characterization of complexes

The chemistry of the complexes were investigated by using the following techniques :

3.4.1 Elemental Analysis

3.4.2 Fast-atom bombardment Mass Spectrometry (FAB-MS)

3.4.3 UV-Visible Absorption Spectroscopy (UV-Vis)

3.4.4 Infrared Spectroscopy (IR)

3.4.5 Nuclear Magnetic Resonance Spectroscopy (NMR; 1D and 2D)

3.4.6 Cyclic Voltammetry (CV)

3.4.7 X-ray Crystallography

3.4.1 Elemental Analysis

The composition of elements in the complexes were studied by elemental analysis. The elemental analysis data of *ctc*-, *cct* and *ttt*-[Ru(bsazpy)$_2$Cl$_2$] complexes are listed in Table 9.

Table 9. Elemental analysis data of the [Ru(bsazpy)$_2$Cl$_2$] complexes

Complexes	% C		% H		% N	
	Calc.	Found	Calc.	Found	Calc.	Found
ctc-[Ru(bsazpy)$_2$Cl$_2$]	48.00	47.95	2.79	2.79	12.92	13.12
cct-[Ru(bsazpy)$_2$Cl$_2$]	48.00	45.92	2.79	2.79	12.92	12.42
ttt-[Ru(bsazpy)$_2$Cl$_2$]	48.00	47.54	2.79	2.62	12.92	12.51

From the elemental analysis data, the analytical values of *ctc*-, *cct*- and *ttt*-[Ru(bsazpy)$_2$Cl$_2$] complexes corresponded to the calculated values. Thus, the composition of elements in the complexes were confirmed by this technique.

3.4.2 Fast-Atom Bombardment (FAB) Mass Spectrometry

The molecular weights of the complexes were investigated by FAB mass spectrometry. The FAB mass spectra of *ctc*- and *cct*-[Ru(bsazpy)$_2$Cl$_2$] complexes are shown in Figure 15 and Figure 16. The FAB-Mass spectrometric data with the corresponding relative abundance are summarized in Table 10.

Table 10. FAB mass spectrometric data of the [Ru(bsazpy)$_2$Cl$_2$] complexes

Complexes	m/z	Stoichiometry	Equivalent Species	Rel. Abun. (%)
ctc-[Ru(bsazpy)$_2$Cl$_2$]	615	[Ru(bsazpy)$_2$Cl$_2$-Cl]$^+$	[M-Cl]$^+$	100
	652	[Ru(bsazpy)$_2$Cl$_2$+H]$^+$	[M+H]$^+$	44
cct-[Ru(bsazpy)$_2$Cl$_2$]	615	[Ru(bsazpy)$_2$Cl$_2$-Cl]$^+$	[M-Cl]$^+$	64
	652	[Ru(bsazpy)$_2$Cl$_2$+H]$^+$	[M+H]$^+$	56

M = Molecular weight of the complexes = 650.55 g/mol

FAB mass spectra of these complexes were nearly identical which indeed confirmed that these complexes were isomers.

The peak at m/z 615 was observed in the complexes which corresponded to the molecular weight of $[Ru(bsazpy)_2Cl_2]$ exclusive of one chloride atom. Another peak at m/z 652 was assigned to one protonation of $[Ru(bsazpy)_2Cl_2]$.

Thus, the expected structures of both isomers were supported by this technique.

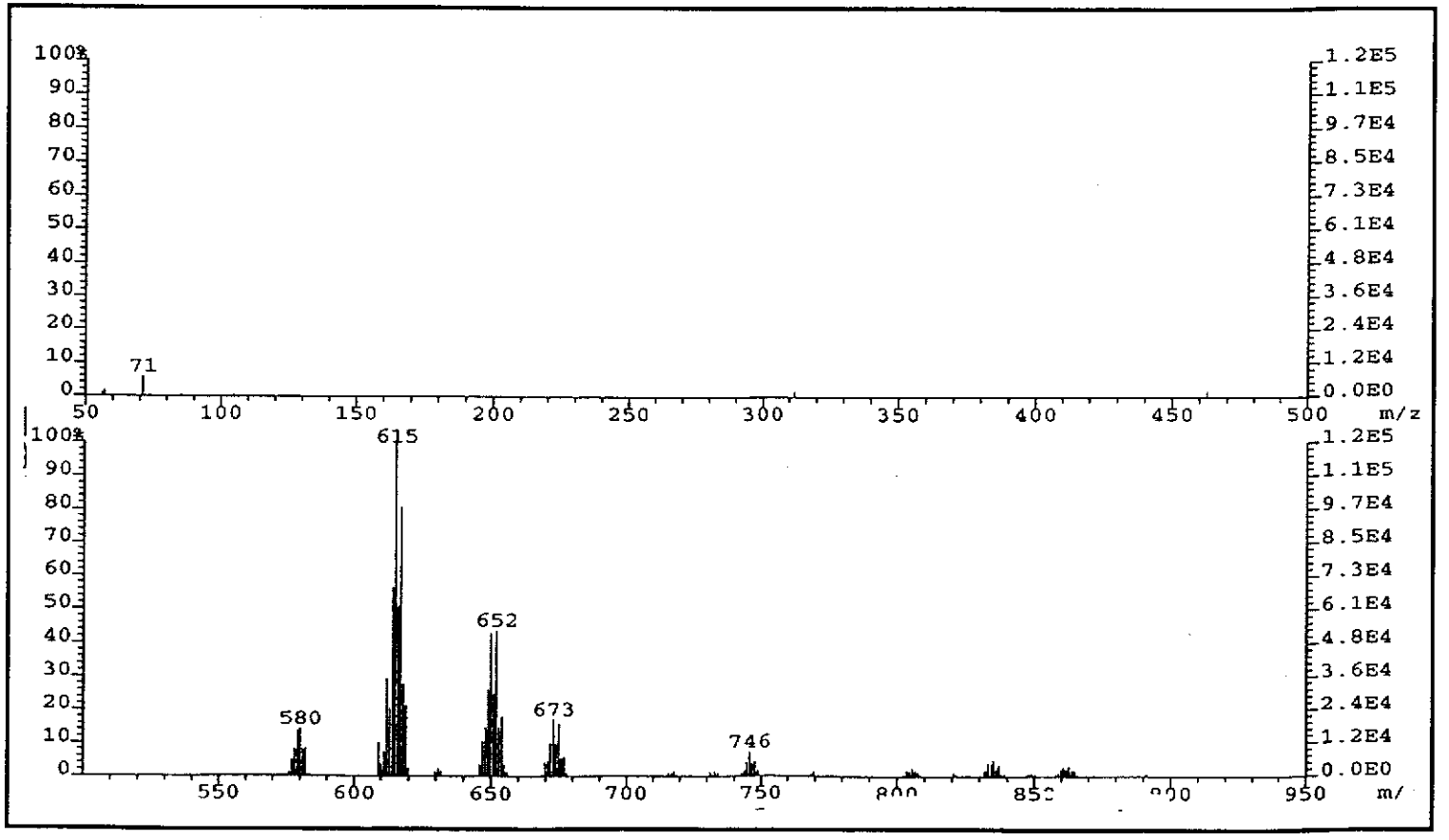

Figure 15. FAB mass spectrum of *ctc*-[$Ru(bsazpy)_2Cl_2$].

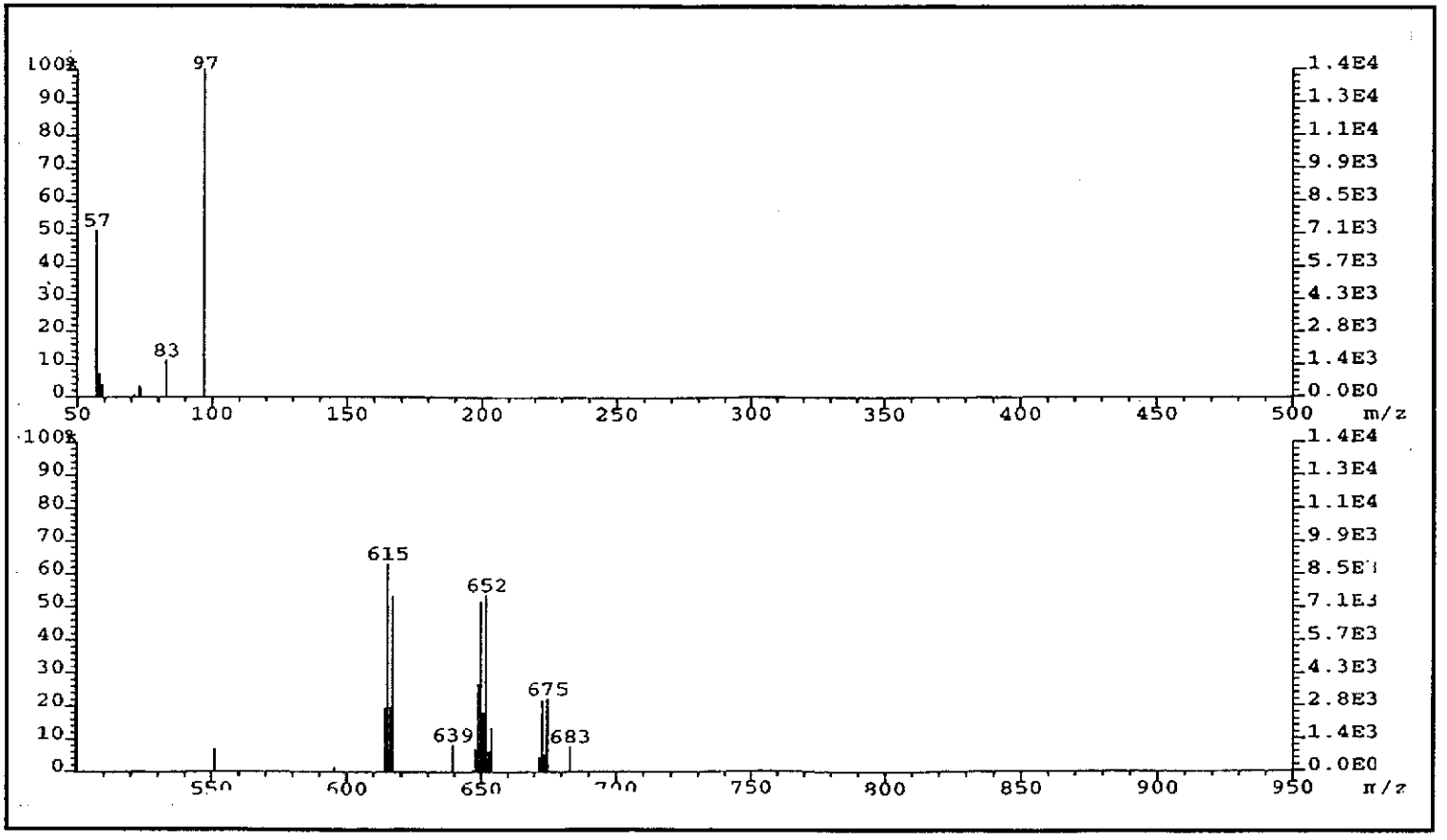

Figure 16. FAB mass spectrum of *cct*-[Ru(bsazpy)$_2$Cl$_2$].

3.4.3 UV-Visible Absorption Spectroscopy

Electronic spectra of the complexes in various solvents were recorded in the range 200-800 nm. The electronic spectral data are collected in Table 11. The absorption spectra of *ctc*-, *cct*- and *ttt*-[Ru(bsazpy)$_2$Cl$_2$] complexes in CH_2Cl_2 are shown in Figure 17 to Figure 19.

Table 11. The electronic spectral data of the [Ru(bsazpy)$_2$Cl$_2$] complexes

Complexes	λ_{max}, nm (10^{-4} ε^a, $M^{-1}cm^{-1}$)				
	CH_2Cl_2	$CHCl_3$	CH_3CN	DMF	DMSO
ctc-[Ru(bsazpy)$_2$Cl$_2$]	404 (3.25) 618 (1.87)	405 (3.31) 619 (1.87)	400 (2.78) 612 (1.56)	403 (2.56) 618 (1.43)	406 (2.89) 617 (1.69)
cct-[Ru(bsazpy)$_2$Cl$_2$]	426 (3.00) 630 (0.78)	428 (3.29) 634 (0.86)	420 (2.41) 626 (0.65)	424 (2.95) 633 (0.80)	426 (3.00) 631 (0.81)
ttt-[Ru(bsazpy)$_2$Cl$_2$]	298 (0.66) 377 (1.04) 645 (0.65)	296 (0.41) 377 (0.63) 649 (0.42)	-	294 (0.45) 386 (0.70) 636 (0.37)	411 (1.02) 614 (0.37)

[a] Molar extinction coefficient

The *ctc*- and the *cct*- [Ru(bsazpy)$_2$Cl$_2$] complexes displayed two absorption bands in the visible region (400-800 nm) with high molar extinction coefficient (ε ~ 6000-33000 $M^{-1}cm^{-1}$). These absorption bands were assigned to the t_2(Ru) $\rightarrow$ π^*(Ligand) MLCT transitions where the π^* orbital had a large azo character (Senapoti, *et al.*, 2002). The spectral patterns of the both isomers of [Ru(bsazpy)$_2$Cl$_2$] were nearly

identical except the differences in band positions and intensities. The *ctc*-isomer showed an intense band in the range 400-410 nm (ε ~ 25000-33000 $M^{-1}cm^{-1}$) and a weak band in the range 610-620 nm (ε ~ 14000-19000 $M^{-1}cm^{-1}$). While the *cct*-isomer displayed the intense band in the range 420-430 nm (ε ~ 24000-33000 $M^{-1}cm^{-1}$) and the weak band in the range 620-640 nm (ε ~ 6000-9000 $M^{-1}cm^{-1}$).

Whereas, the *ttt*- $[Ru(bsazpy)_2Cl_2]$ complex displayed one absorption band at around

295 nm (ε ~ 4000-6000 $M^{-1}cm^{-1}$) which was assigned to intraligand charge transfer transitions and two absorption bands in the visible region which were assigned to the $t_2(Ru) \longrightarrow \pi^*$(Ligand) MLCT transitions.

The energy of the MLCT transition was symmetry-dependent (Santra, *et. al.*, 1999). The less symmetric isomer should exhibit a stronger $d\pi$-$p\pi$ interaction. Both *cis*-isomers which had C_2-symmetry (*ctc*, *cct*) exhibited higly intense MLCT transitions at higher energies compared to *trans*-isomer (*ttt*) which had C_{2h}-symmetry.

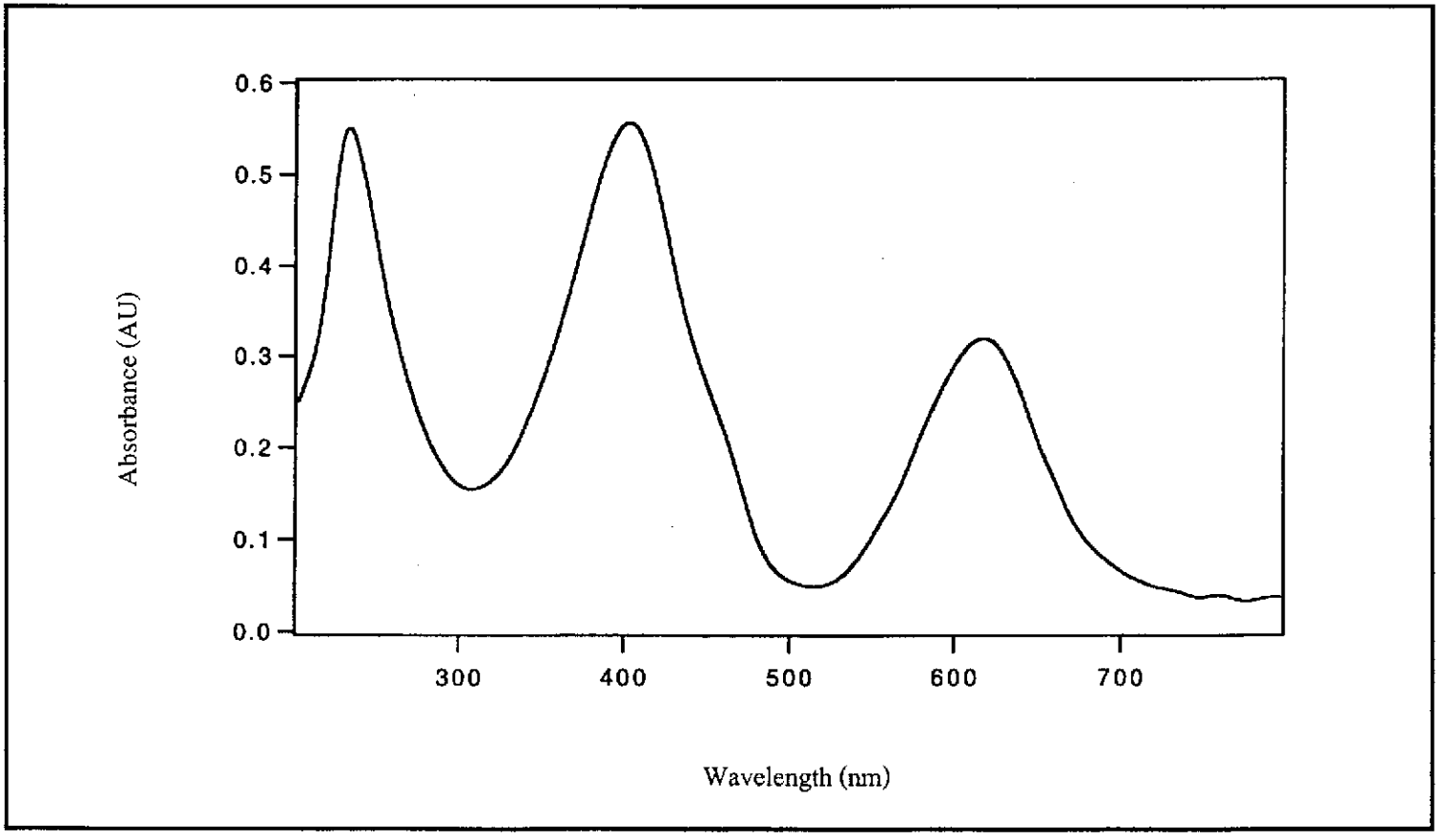

Figure 17. UV-Visible absorption spectrum of *ctc*-[$Ru(bsazpy)_2Cl_2$] in CH_2Cl_2.

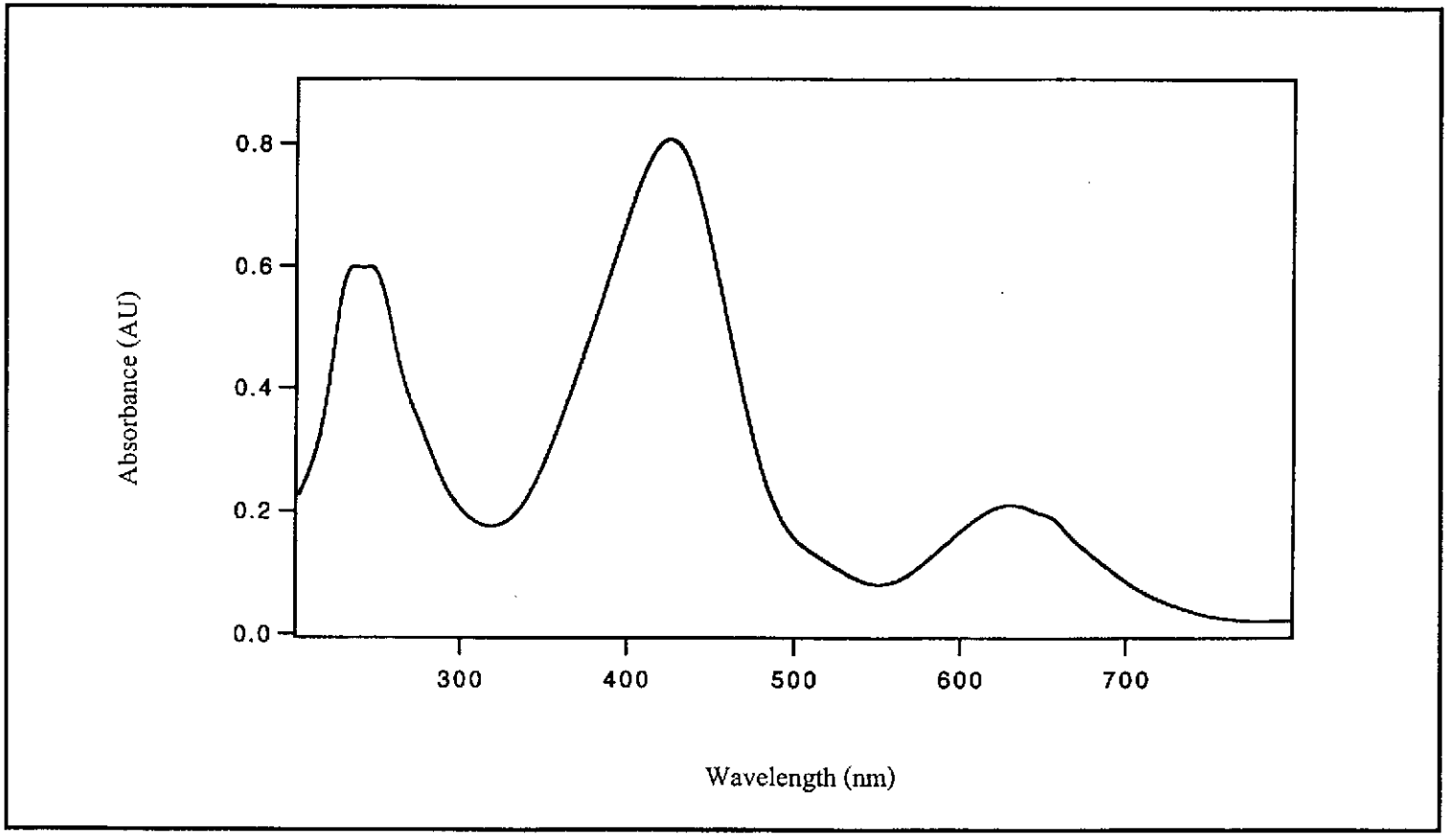

Figure 18. UV-Visible absorption spectrum of *cct*-[Ru(bsazpy)$_2$Cl$_2$] in CH_2Cl_2.

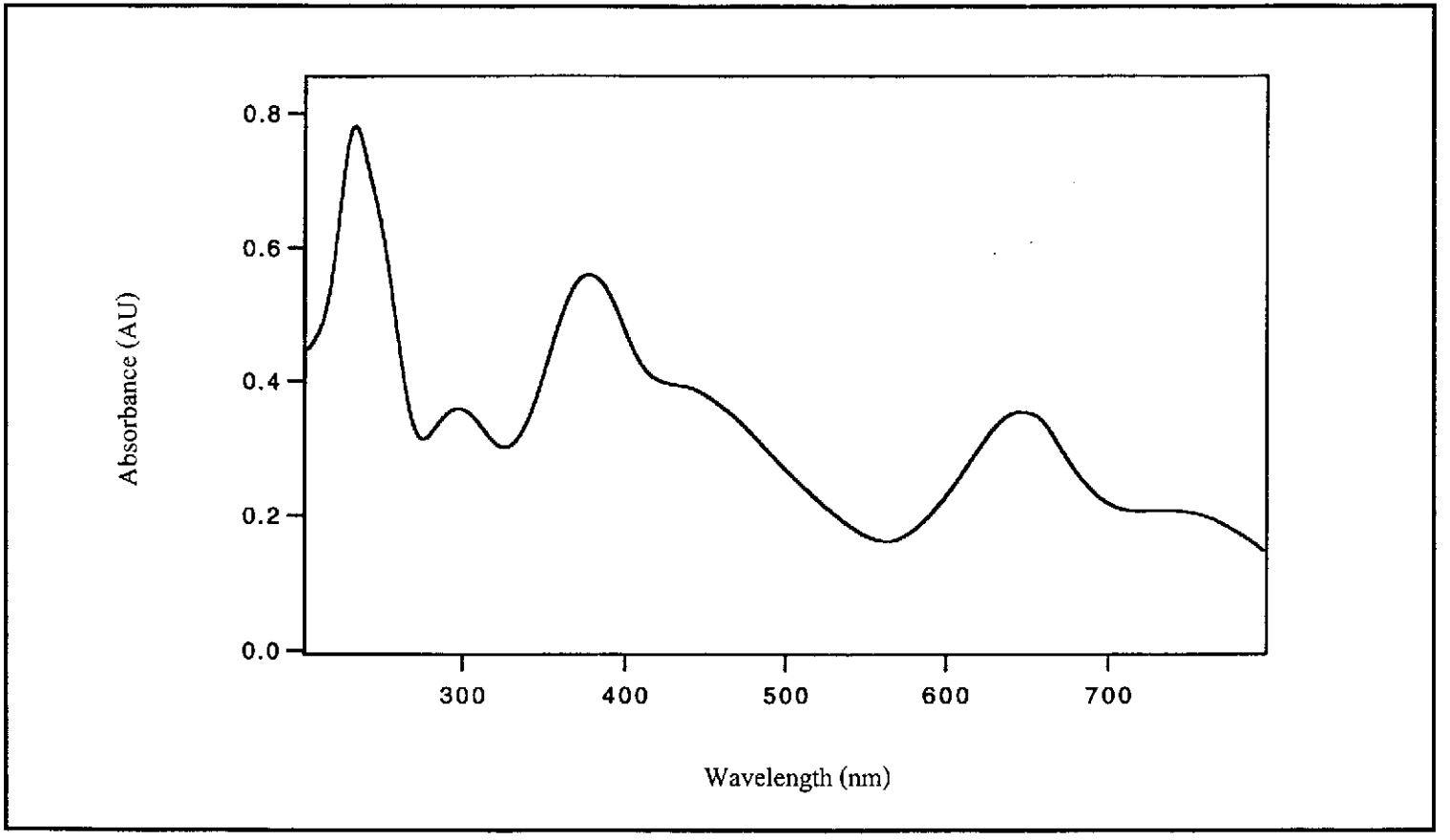

Figure 19. UV-Visible absorption spectrum of *ttt*-[$Ru(bsazpy)_2Cl_2$] in CH_2Cl_2.

3.4.4 Infrared Spectroscopy

Infrared spectroscopy is an useful technique to study the important functional group in the compounds. Infrared spectra of *ctc*-, *cct*- and *ttt*-[Ru(bsazpy)$_2$Cl$_2$] are recorded in the range 4000-400 cm^{-1} and shown in Figure 20 to Figure 22. The selected infrared spectroscopic data of the complexes are collected in Table 12 and compared with the free bsazpy ligand.

Table 12. The selected IR spectroscopic data of the bsazpy ligand and the [Ru(bsazpy)$_2$Cl$_2$] complexes

Vibration modes	Frequencies (cm^{-1})			
	bsazpy	*ctc*-isomer	*cct*-isomer	*ttt*-isomer
C=N, C=C stretching	1491 (m) 1458 (s)	1454 (m) 1373 (m) 1317 (s)	1440 (m) 1381 (w) 1322 (s)	1457 (m) 1321 (w) 1277 (s)
N=N stretching	1317 (s)	1266 (s) 1244 (s)	1240 (s)	1234 (s)
C-H bending of monosubstituted benzene	757 (s) 728 (s) 680 (s)	758 (s) 724 (m) 691 (s)	765 (s) 732 (s) 680 (s)	767 (s) 749 (s) 696 (s)

s = strong, m = medium, w = weak

From the spectra of three isomers, the C=N and C=C stretching modes were observed in the range 1300-1500 cm^{-1}. The peaks which appeared in the range 650-800 cm^{-1} were assigned to the characteristic of the monosubstituted benzene.

The most important peak was N=N stretching mode which used for considering the π-acid property in azo compounds. The sharp peak for N=N stretching at 1317 cm^{-1} in the free bsazpy ligand was shifted to 1230-1266 cm^{-1} in the complexes. The red shift indicated the less double-bond character in the N=N group which was strong evidence for substantial π-backbonding to ruthenium through an azo nitrogen. In the case of $[Ru(azpy)_2Cl_2]$ complexes (Krause and Krause, 1980), the N=N stretching was observed at higher frequencies than that of $[Ru(bsazpy)_2Cl_2]$ complexes. The results from these data supported the π-acceptor property of the bsazpy ligand which was better than the azpy ligand.

Moreover, the IR specta of the *ctc*- and the *cct*-$[Ru(bsazpy)_2Cl_2]$ isomers showed a minor differences in N=N stretching peak. The *ctc*-isomer exhibited two N=N stretching peaks at 1266 and 1244 cm^{-1} whereas the *cct*-isomer showed one peak. These data corresponded to the X-ray crystallographic study which showed that the two N=N bond distances in *ctc*-isomer were non-equivalent but they were equivalent in *cct*-isomer.

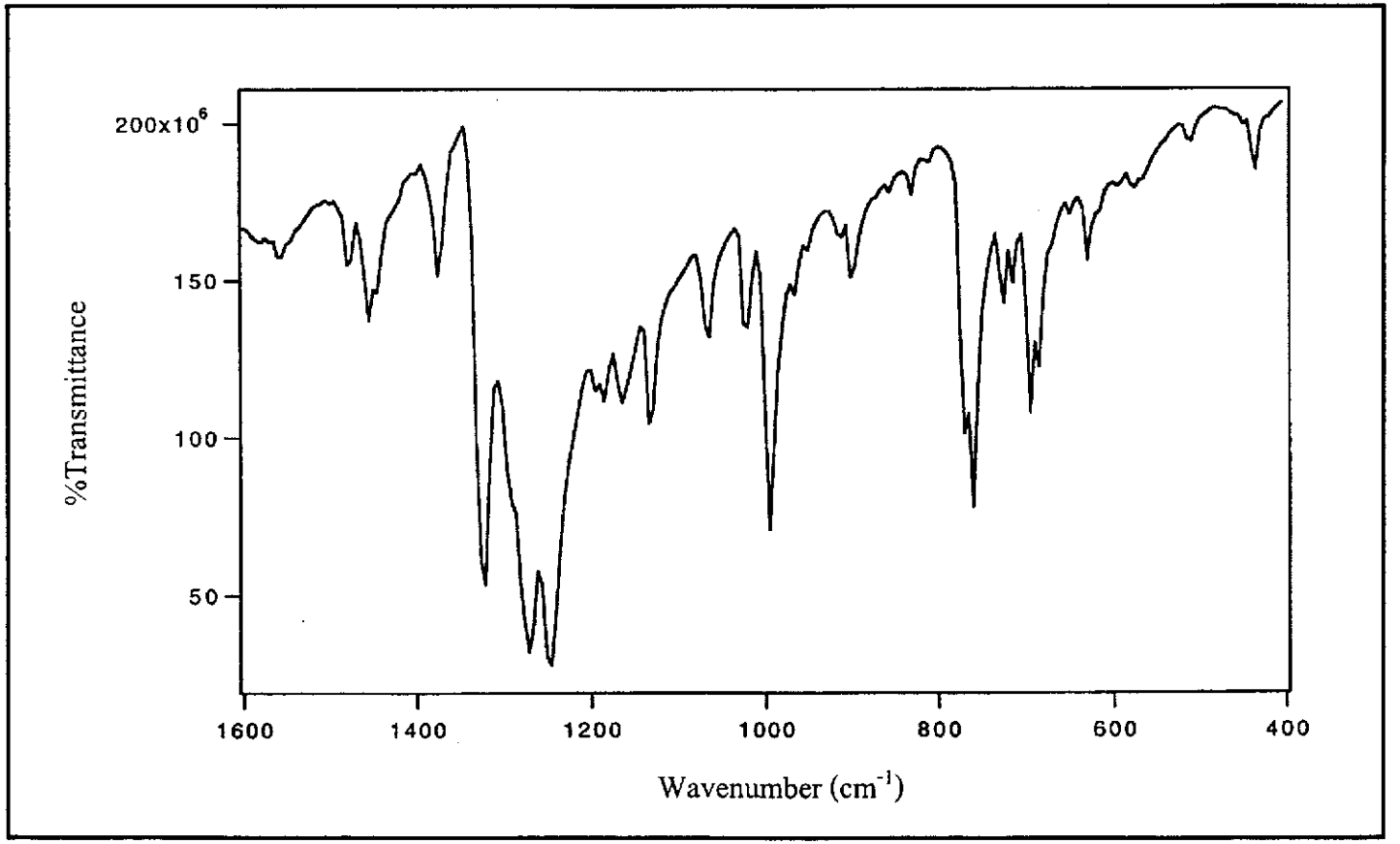

Figure 20. IR spectrum of *ctc*-$[Ru(bsazpy)_2Cl_2]$.

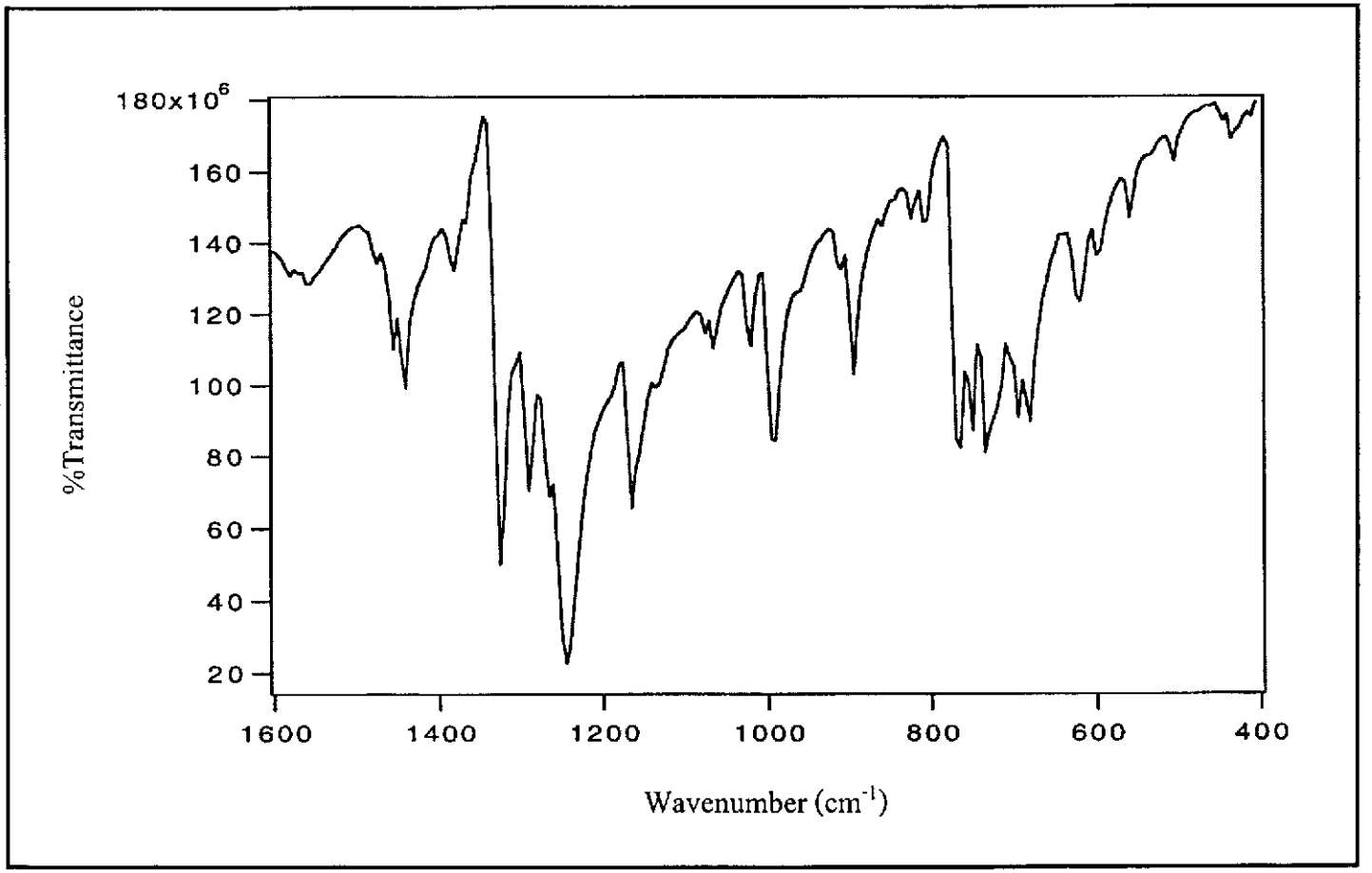

Figure 21. IR spectrum of *cct*-[Ru(bsazpy)$_2$Cl$_2$].

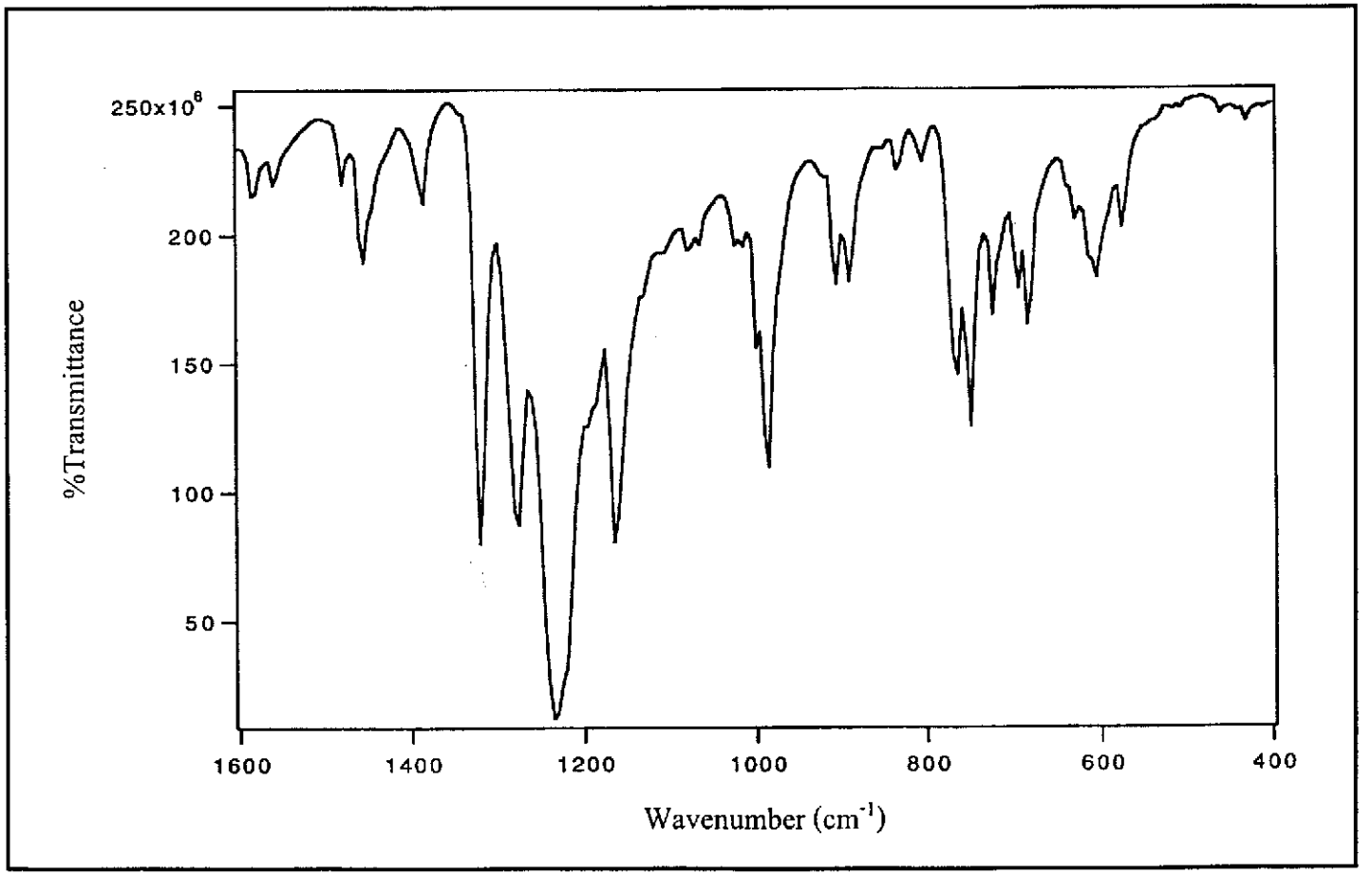

Figure 22. IR spectrum of *ttt*-[Ru(bsazpy)$_2$Cl$_2$].

3.4.5 Nuclear Magnetic Resonance Spectroscopy

The NMR experiments of *ctc*-, *cct*- and *ttt*-[Ru(bsazpy)$_2$Cl$_2$] were carried out in $CDCl_3$ at 500 MHz. The ^{1}H NMR signals were assigned on the basis of spin-spin interaction, comparative integration, coupling constants and ^{1}H-^{1}H COSY NMR spectroscopy. The results from DEPT NMR and ^{1}H-^{13}C NMR spectroscopy supported the ^{13}C NMR assignments. The NMR spectroscopic studies of each complex were described below.

(a) *ctc*-[Ru(bsazpy)$_2$Cl$_2$] complex

The spectral data of the *ctc*-isomer are listed in Table 13 and the atom numbering scheme is shown in Figure 23.

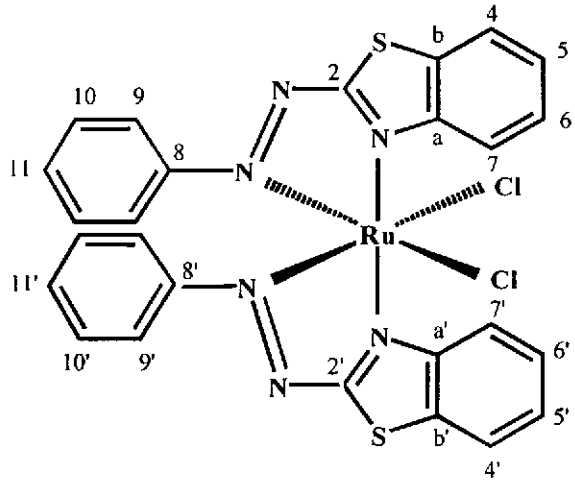

Figure 23. The atom numbering scheme of *ctc*-[Ru(bsazpy)$_2$Cl$_2$].

Table 13. ^{1}H NMR and ^{13}C NMR spectroscopic data of *ctc*-[Ru(bsazpy)$_2$Cl$_2$]

Positions	^{1}H NMR			^{13}C NMR
	δ(ppm)	J (Hz)	Number of H	δ(ppm)
7,7′	8.97 (d)	8.29	1	126.18
4,4′	7.90 (d)	8.05	1	122.24
5,5′	7.49 (t)	7.57	1	127.78
6,6′	7.38 (t)	7.30	1	128.58
11,11′	7.12 (t)	7.45	1	130.27
10,10′	6.94 (t)	7.93	2	128.54
9,9′	6.77 (dd)	8.67, 1.10	2	122.42
2	-	-	-	174.19
a	-	-	-	156.49
b	-	-	-	149.35
8	-	-	-	136.52

d = doublet, t = triplet, dd = doublet of doublet

The ^{1}H NMR spectrum of the *ctc*-isomer (Figure 24) showed only one set of the bsazpy ligand signals, which indicated that the two bsazpy ligands in this isomer were magnetically equivalent with C_2-symmetry.

The spectral pattern of the *ctc*-isomer differed from that of the free bsazpy ligand. The benzothiazole protons (H4(4′) – H7(7′)) were shifted to the downfield side and the phenyl protons (H9(9′) – H11(11′)) were shifted to upfield side (6.70-7.20 ppm) compared to the free ligand values. The doublet at the most downfield position (8.97 ppm) referred to proton H7(7′) because of the closest position to nitrogen atom on the

benzothiazole ring which coordinated the metal center followed by the proton H4(4′) (7.90 ppm). The proton H5(5′) and H6(6′) showed triplet at 7.49 and 7.38 ppm, respectively. The assignments corresponded to the results from ^{1}H-^{1}H COSY NMR spectrum (Figure 25).

The ^{13}C NMR spectrum (Figure 26) of the *ctc*-isomer displayed 11 carbon resonances. The ^{13}C NMR assignments were supported by the results from ^{1}H-^{13}C HMQC NMR spectrum, which is shown in Figure 28. The most downfield resonance at 174.19 ppm was assigned to the quaternary carbon C2(2′). The signals of other quaternary carbons, Ca(a′), Cb(b′) and C8(8′) appeared at 156.49, 149.35 and 136.52 ppm, respectively. The methine carbon resonances appeared in the range 120-131 ppm which corresponded to the results from DEPT NMR spectrum (Figure 27).

Thus, the NMR data supported the structure of *cis-trans-cis*-$[Ru(bsazpy)_2Cl_2]$.

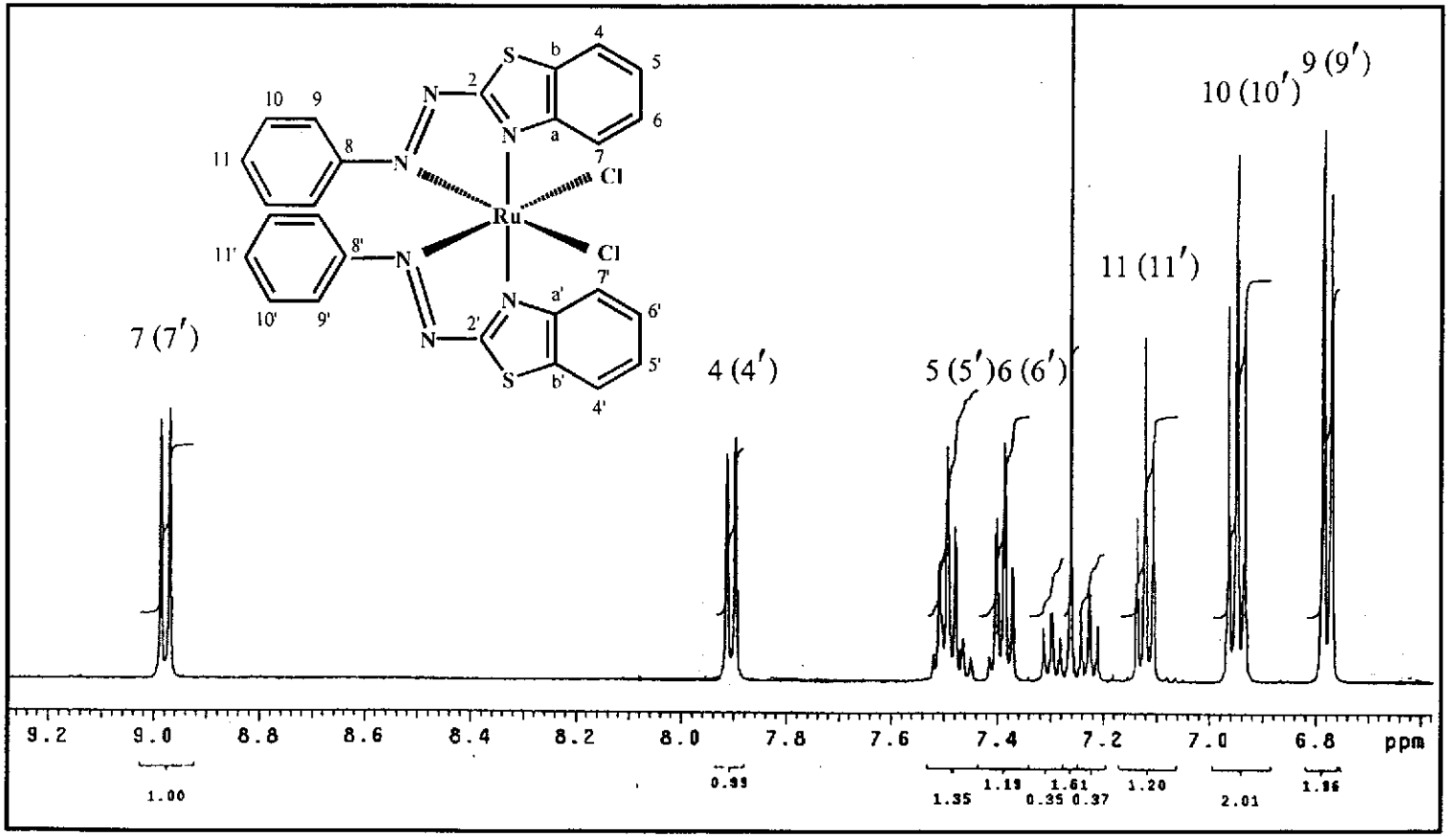

Figure 24. ^{1}H NMR spectrum of *ctc*-[Ru(bsazy)$_2$Cl$_2$] in CDCl$_3$ (500 MHz).

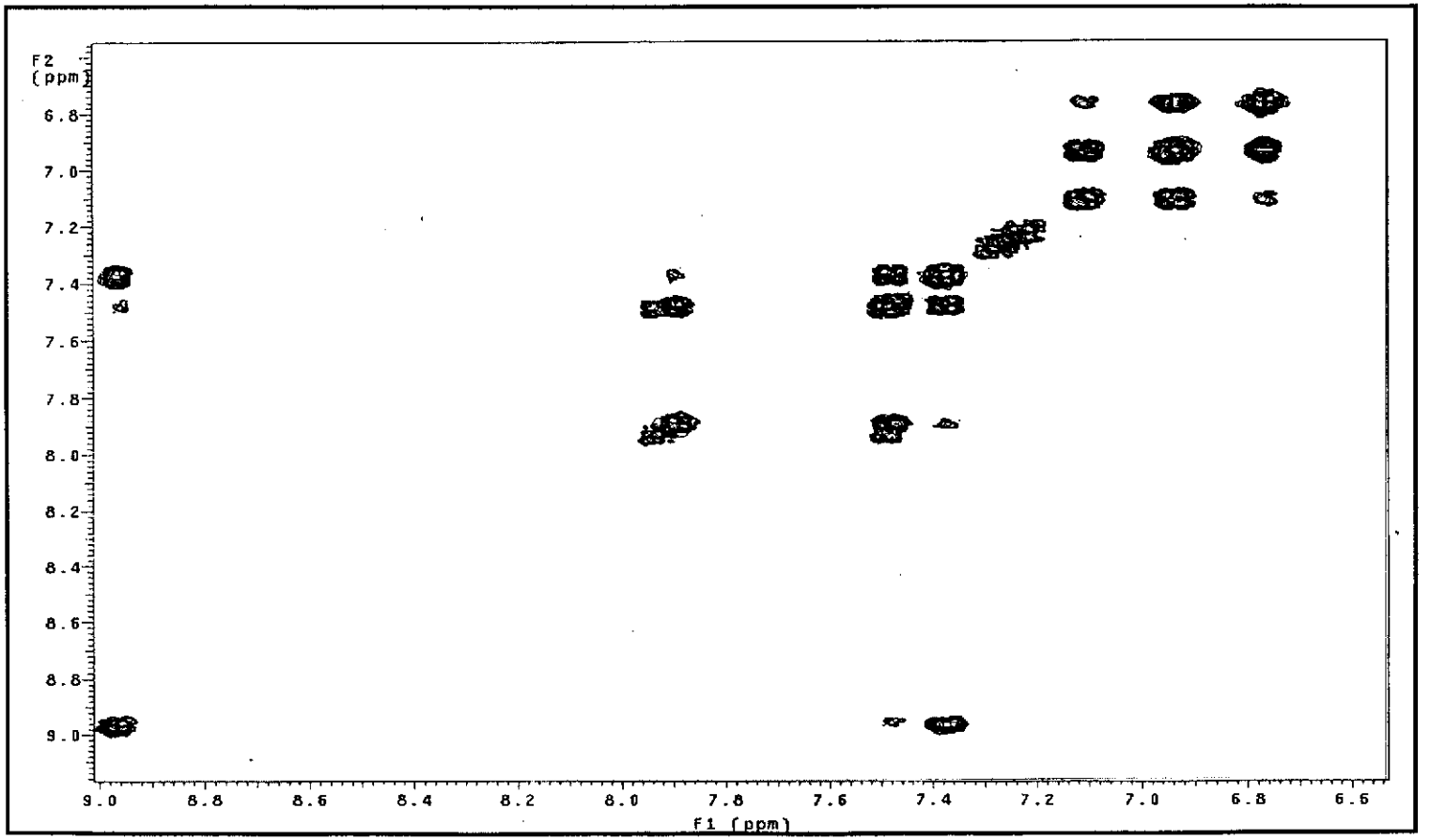

Figure 25. ^{1}H-^{1}H COSY NMR spectrum of *ctc*-$[Ru(bsazy)_2Cl_2]$ in $CDCl_3$ (500 MHz).

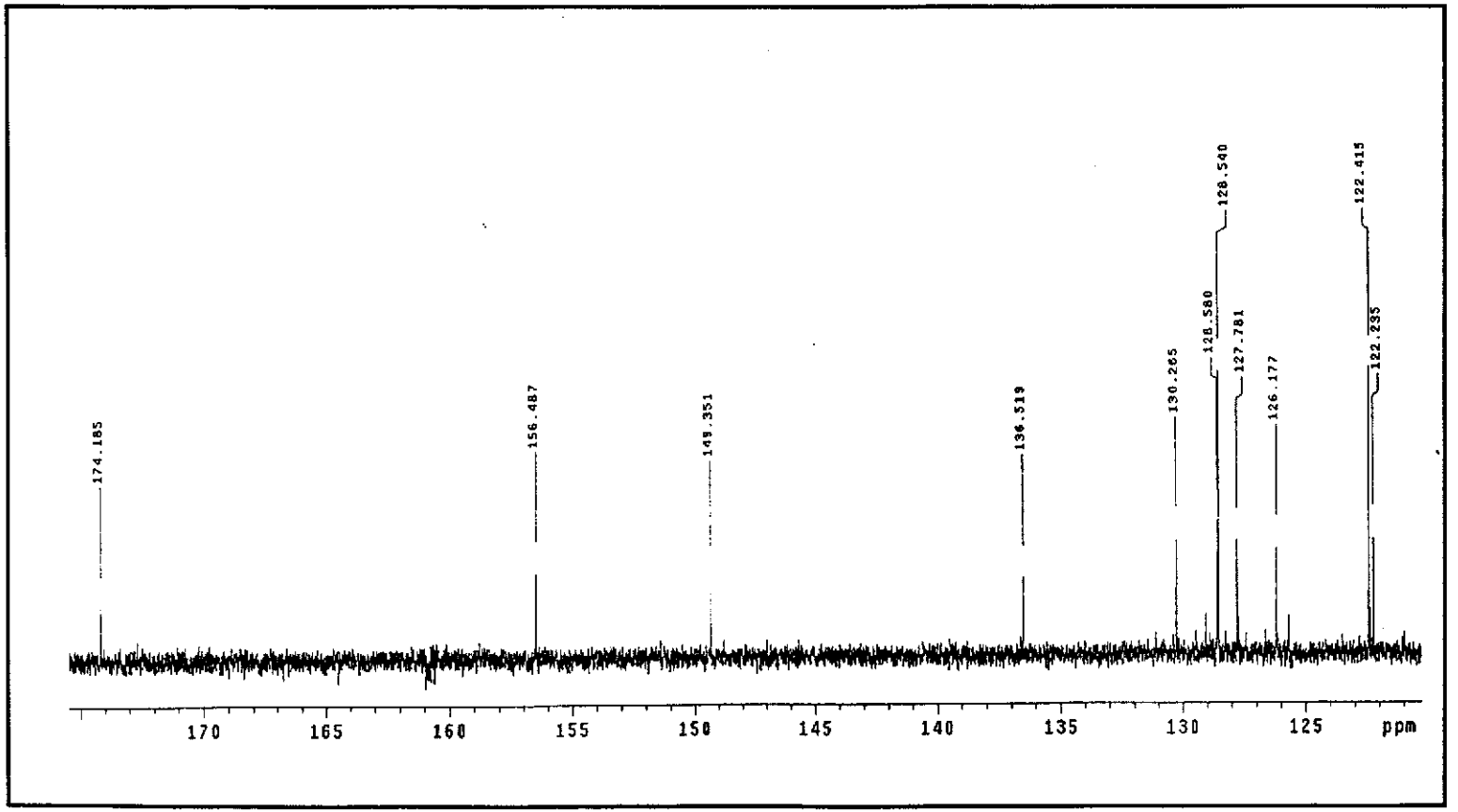

Figure 26. ^{13}C NMR spectrum of *ctc*-$[Ru(bsazy)_2Cl_2]$ in $CDCl_3$ (500 MHz).

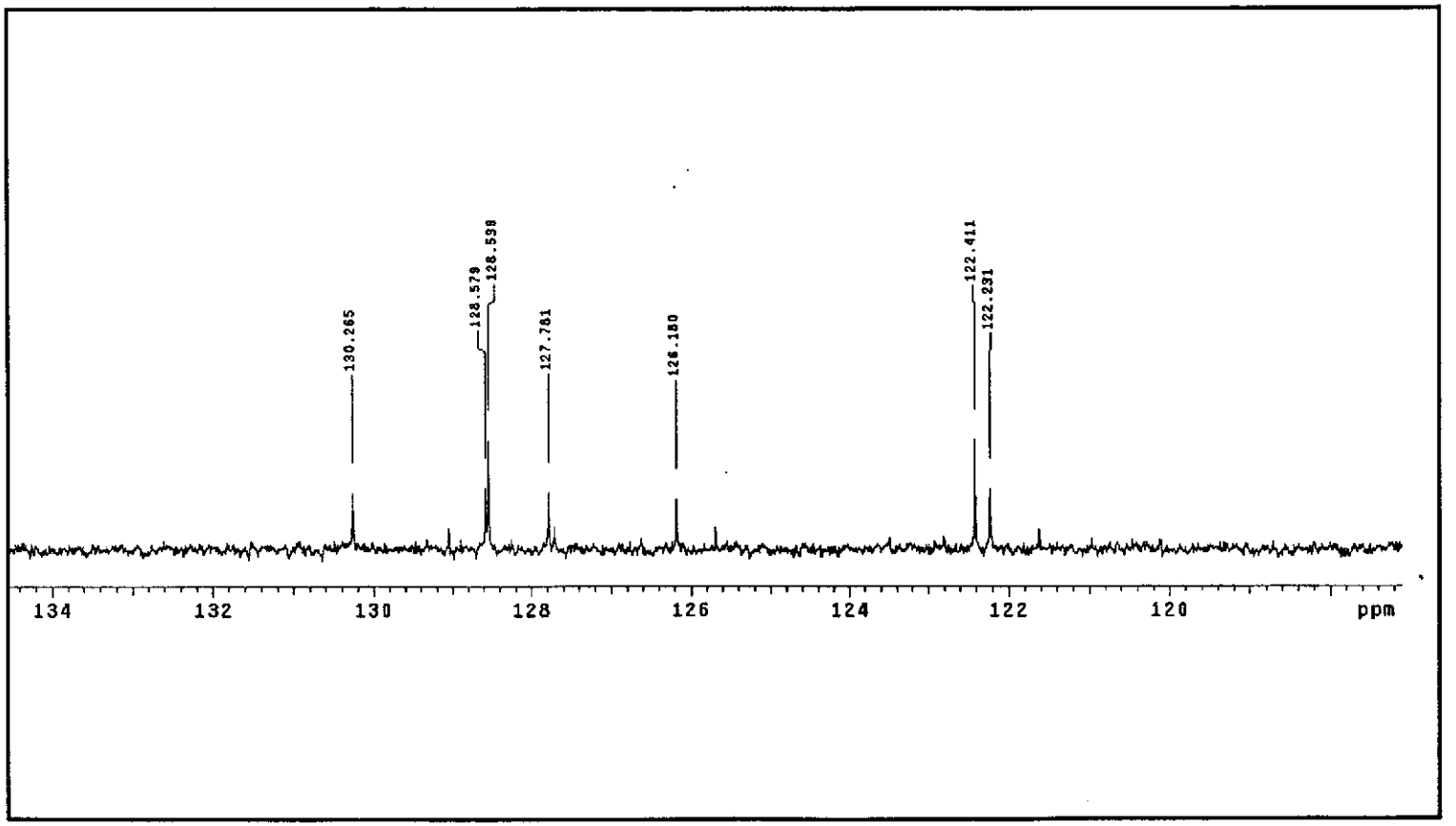

Figure 27. DEPT NMR spectrum of *ctc*-[Ru(bsazy)$_2$Cl$_2$] in CDCl$_3$ (500 MHz).

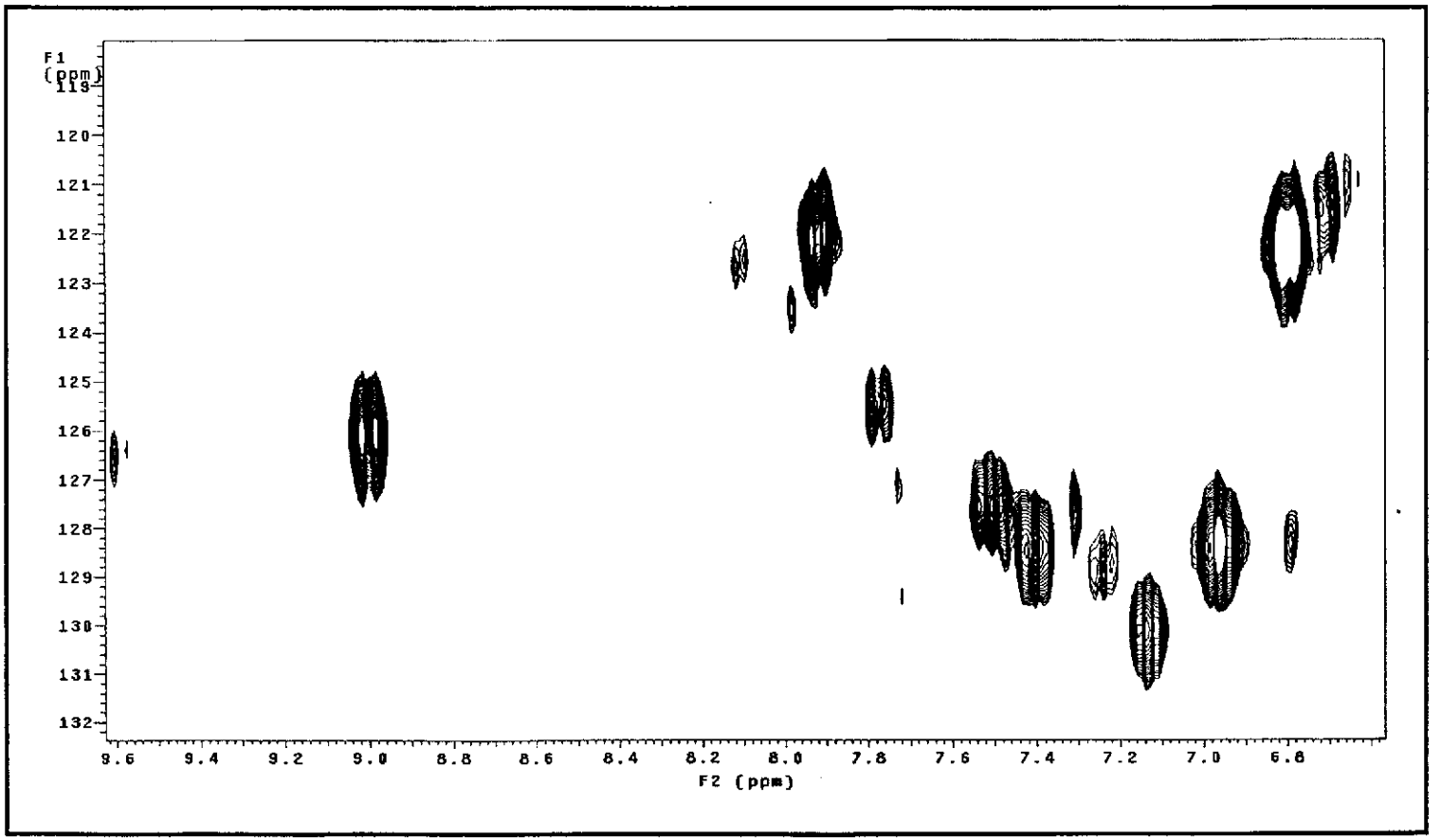

Figure 28. ^{1}H- ^{13}C HMQC NMR spectrum of *ctc*-$[Ru(bsazy)_2Cl_2]$ in $CDCl_3$ (500 MHz).

(b) *cct*-[Ru(bsazpy)$_2$Cl$_2$] complex

The chemical shift data of the *cct*-isomer are collected in Table 14 and the atom numbering scheme is shown in Figure 29.

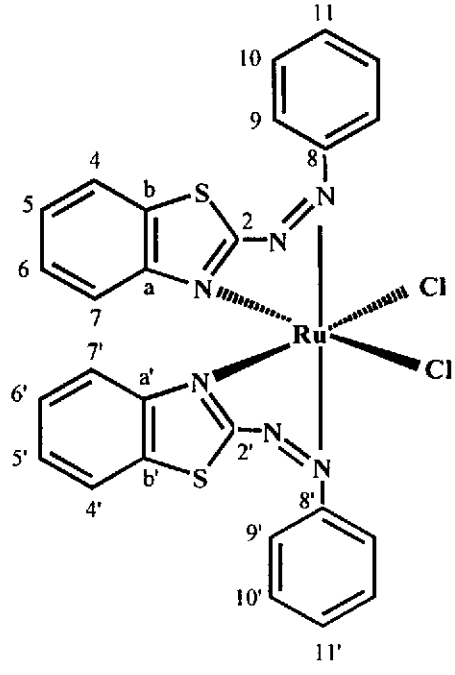

Figure 29. The atom numbering scheme of *cct*-[Ru(bsazpy)$_2$Cl$_2$].

Table 14. ^{1}H NMR and ^{13}C NMR spectroscopic data of *cct*-[Ru(bsazpy)$_2$Cl$_2$]

Positions	^{1}H NMR			^{13}C NMR
	δ(ppm)	J (Hz)	Number of H	δ(ppm)
9,9′	8.22(d)	7.81	2	127.01
7,7′	7.94 (d)	8.05	1	123.65
11,11′	7.59 (t)	7.33	1	131.91
6,6′	7.50 (t)	7.32	1	128.30
10,10′	7.44 (t)	7.69	2	128.18
5,5′	7.32 (t)	7.69	1	128.24
4,4′	7.05 (d)	8.29	1	121.63
2	-	-	-	173.52
a	-	-	-	156.76
b	-	-	-	156.72
8	-	-	-	135.96

d = doublet, t = triplet

Similar to the *ctc*-isomer, the ^{1}H NMR spectrum of the *cct*-isomer (Figure 30) showed only one set of bsazpy ligand signals, which indicated that the two bsazpy ligands in this isomer were magnetically equivalent with C_2-symmetry.

The ^{1}H NMR spectrum of the *cct*-isomer showed 7 proton resonances. The spectral pattern of the *cct*-isomer differed from that of the free bsazpy ligand and the *ctc*-isomer. The doublet at the most downfield position (8.22 ppm) referred to proton H9(9′) because of the *trans*-configuration of two azo groups in the molecule and the proton

H7(7′) appeared at 7.94 ppm. The proton H11(11′), H6(6′), H10(10′) and H5(5′) showed triplet at 7.59, 7.50, 7.44, and 7.32 ppm, respectively. The doublet at the most highfield position (7.05 ppm) referred to proton H4(4′). The assignments corresponded to the results from ^{1}H-^{1}H COSY NMR spectrum (Figure 31).

The ^{13}C NMR spectrum (Figure 32) of *cct*-isomer showed 11 carbon resonances. The most downfield resonance at 173.52 ppm was assigned to the quaternary carbon C2(2′). The signals of other quaternary carbons, Ca(a′), Cb(b′) and C8(8′) appeared at 156.76, 156.72 and 135.96 ppm, respectively. The methine carbon signals appeared in the range 120-131 ppm which supported by the results from DEPT NMR spectrum (Figure 33). The ^{13}C NMR assignments corresponded to the results from ^{1}H-^{13}C HMQC NMR spectrum, which is shown in Figure 34.

Therefore, the structure of *cis-cis-trans*-[Ru(bsazpy)$_2$Cl$_2$] was supported by NMR data.

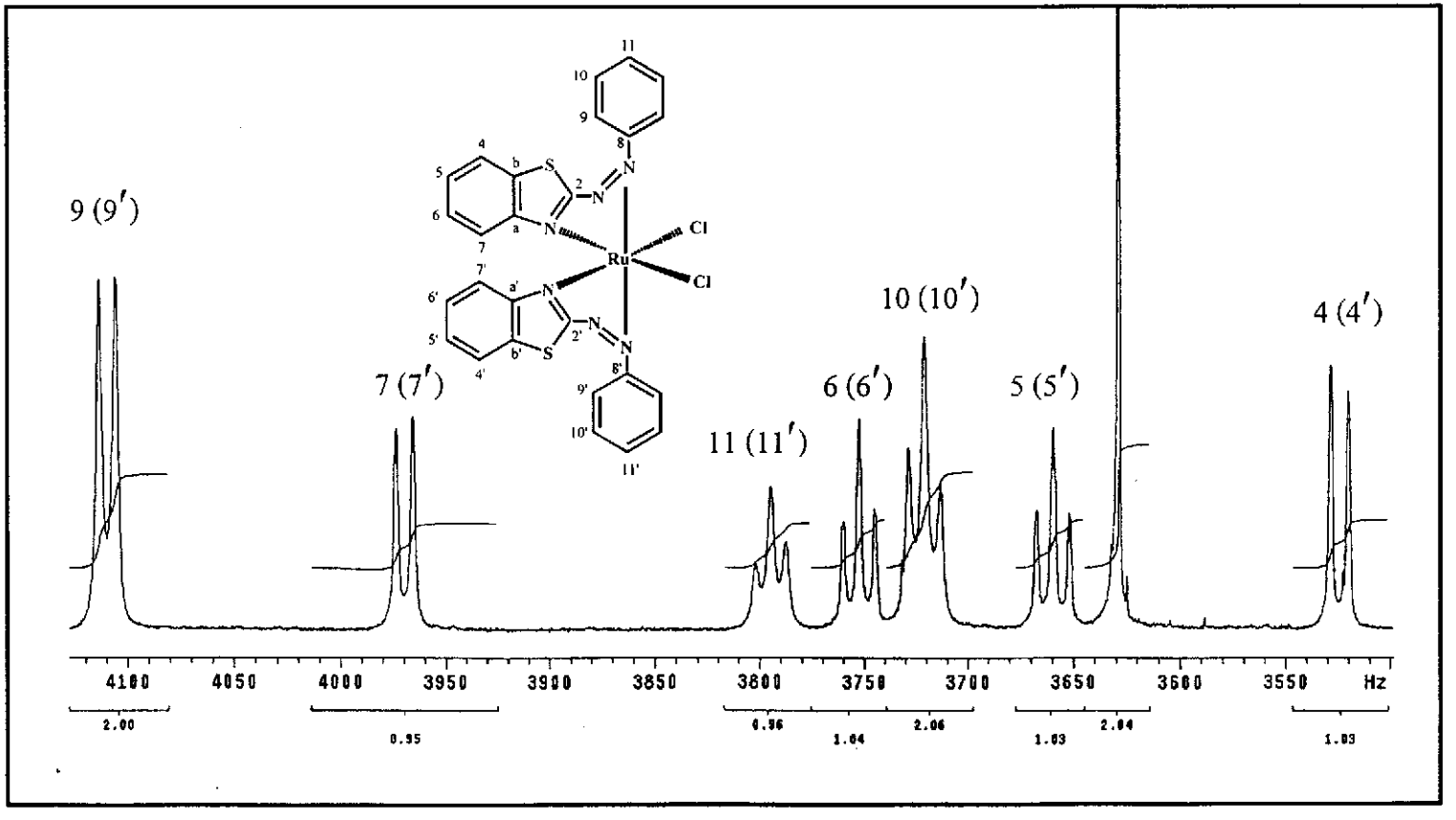

Figure 30. ^{1}H NMR spectrum of *cct*-$[Ru(bsazy)_2Cl_2]$ in $CDCl_3$ (500 MHz).

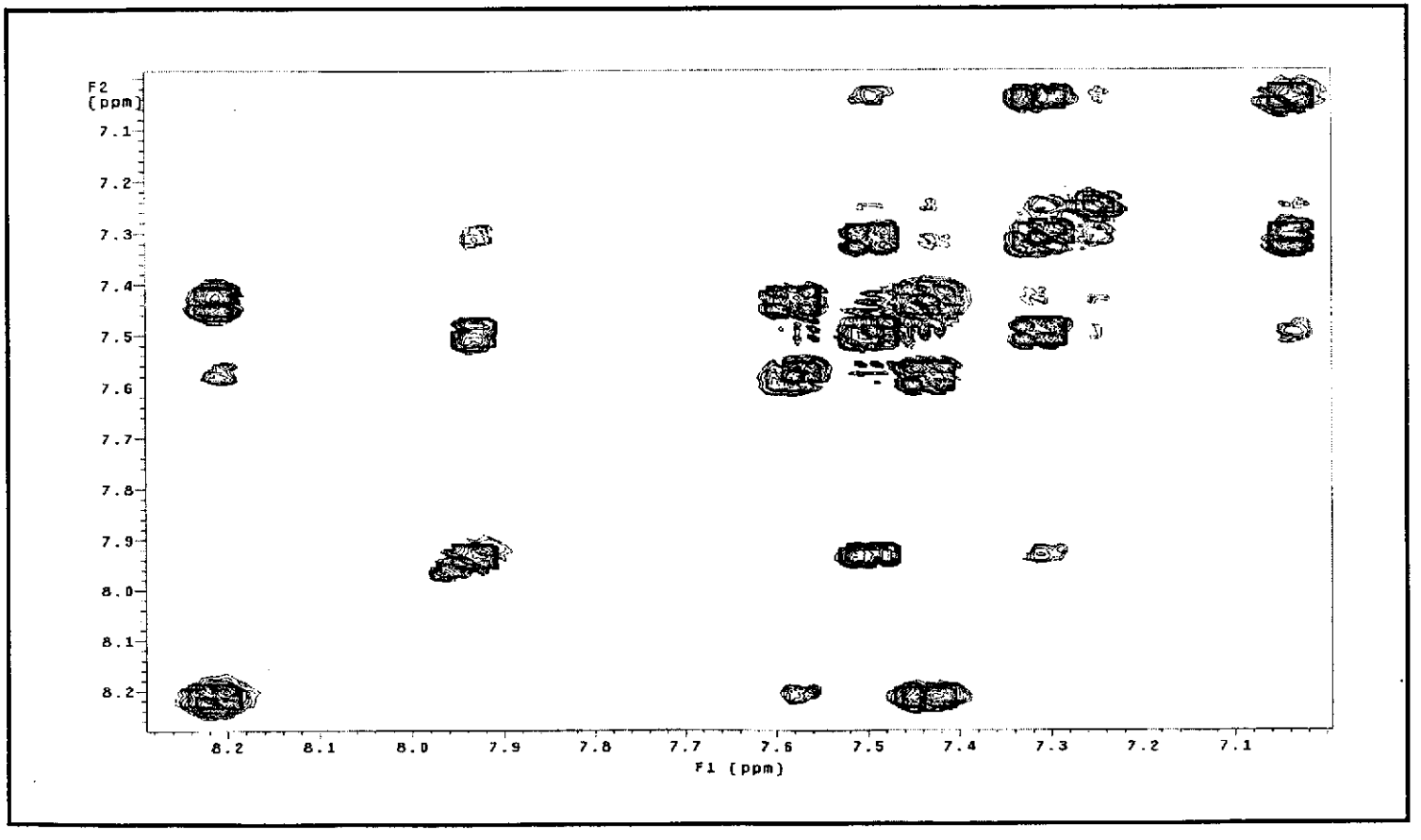

Figure 31. ^{1}H-^{1}H COSY NMR spectrum of *cct*-[$Ru(bsazy)_2Cl_2$] in $CDCl_3$ (500 MHz).

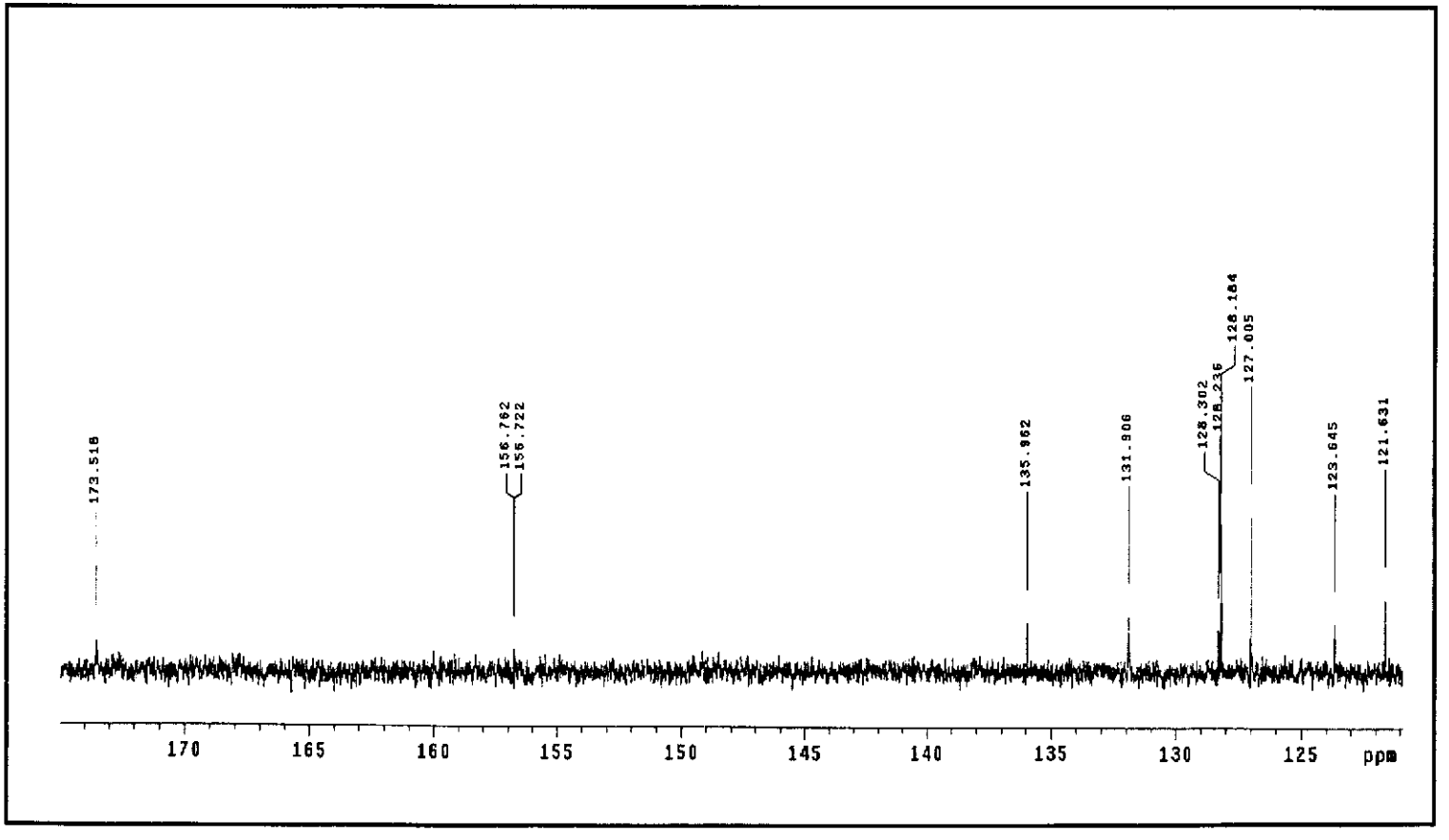

Figure 32. ^{13}C NMR spectrum of *cct*-[Ru(bsazy)$_2$Cl$_2$] in $CDCl_3$ (500 MHz).

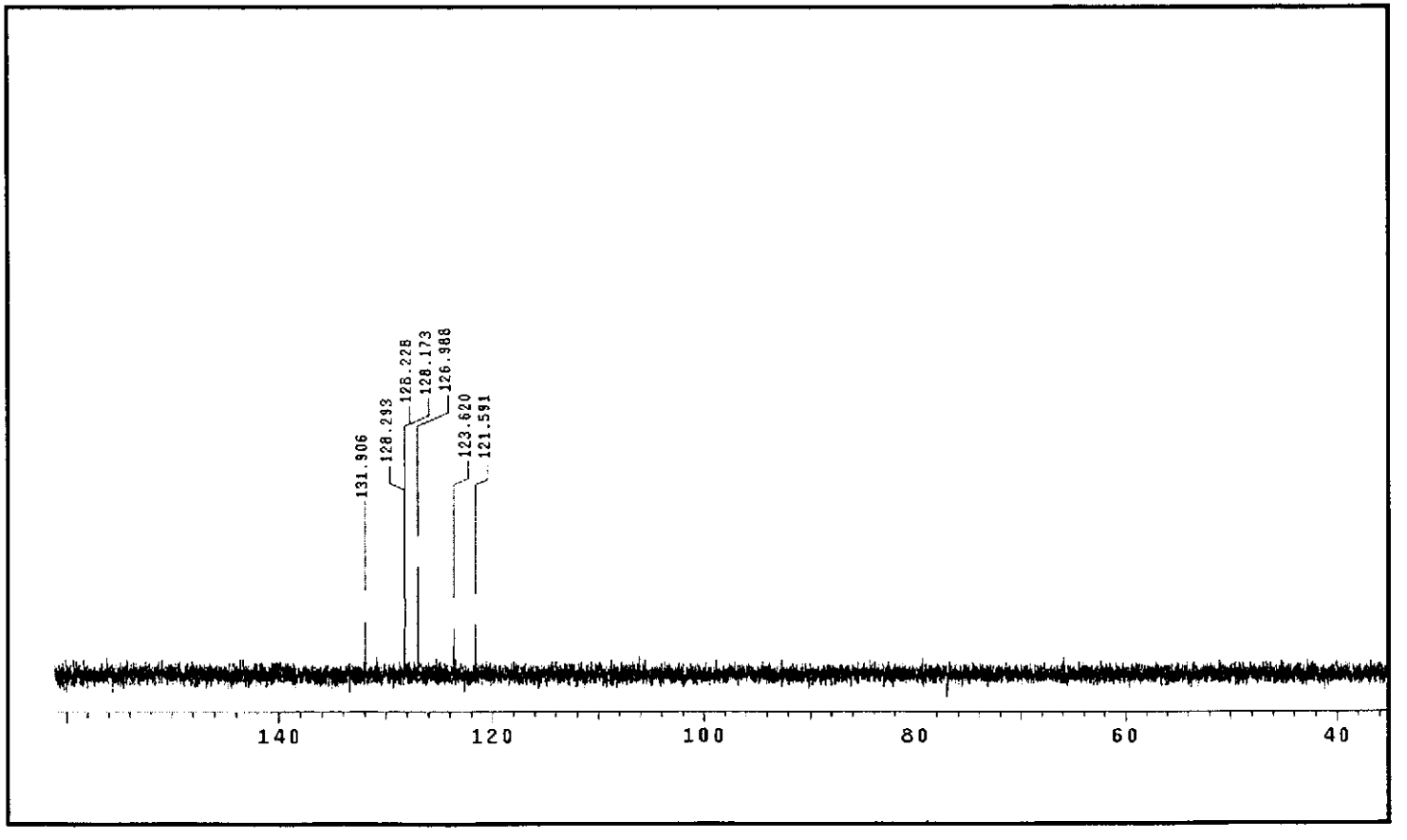

Figure 33. DEPT NMR spectrum of *cct*-[$Ru(bsazy)_2Cl_2$] in $CDCl_3$ (500 MHz).

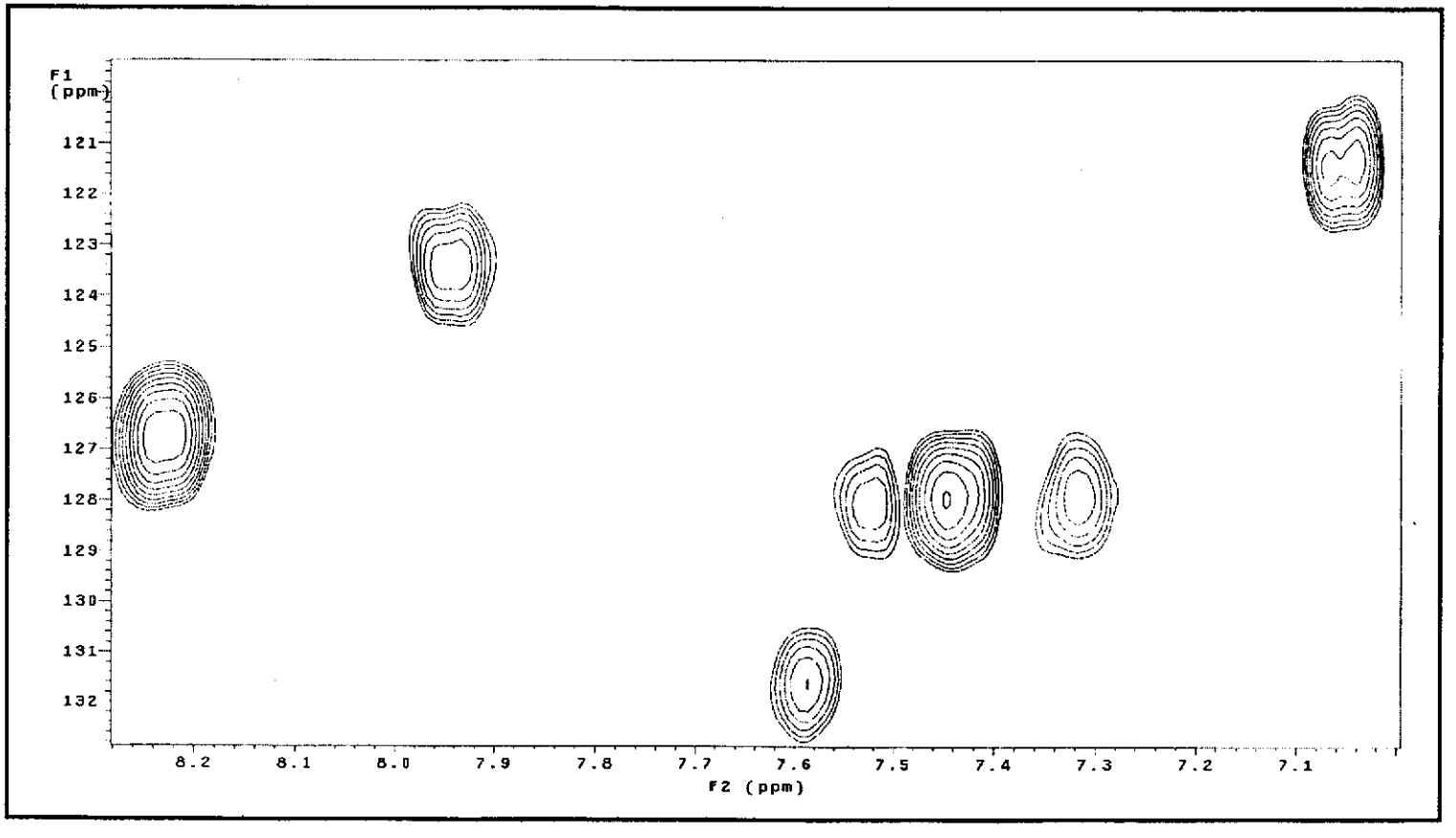

Figure 34. ^{1}H- ^{13}C HMQC NMR spectrum of *cct*-[$Ru(bsazy)_2Cl_2$] in $CDCl_3$ (500 MHz).

(c) *ttt*-[Ru(bsazpy)$_2$Cl$_2$] complex

The spectral data of the *ttt*-isomer are listed in Table 15 and the atom numbering scheme is shown in Figure 35.

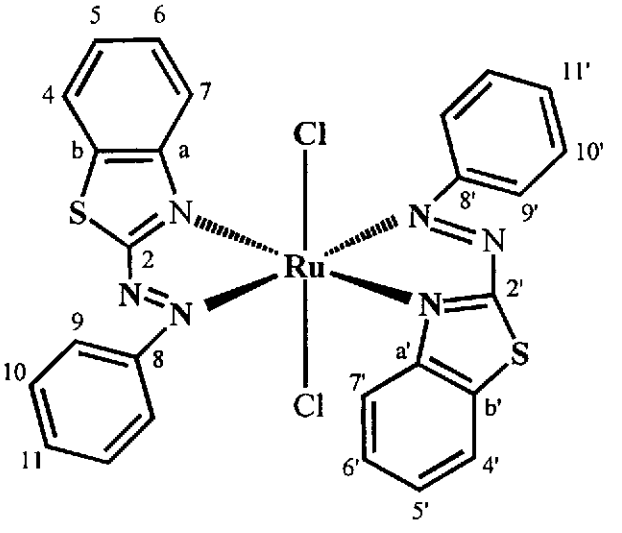

Figure 35. The atom numbering scheme of *ttt*-[Ru(bsazpy)$_2$Cl$_2$].

The NMR spectra of *ttt*-[Ru(bsazpy)$_2$Cl$_2$] were more complicated than that of both *cis*-isomer. Thus, assignment of individual protons were made by ^{1}H-^{1}H COSY coupling, comparative integration, chemical shift data and comparison with the spectrum patterns of the *ctc*-and the *cct*-isomers.

Due to the unsymmetric nature of the bsazpy ligand, there were five geometrical possibilities for [Ru(bsazpy)$_2$Cl$_2$] as *ttt*, *tcc*, *ccc*, *cct* and *ctc* with coordinating pairs in the order Cl, N (N(benzothiazole)), and N' (N(azo)). In this work the structures of the *ctc*- and the *cct*-isomers were confirmed by X-ray crystallography. Thus, *ttt*, *tcc* and *ccc* geometries were possible.

If this complex has *ccc*-configuration, it will show the two sets of ligand signals with C_1-symmetry. But the ^{1}H NMR spectrum of this isomer (Figure 36) showed only one set of the bsazpy ligand signals, which indicated that the two bsazpy ligands in this isomer were magnetically equivalent. So the *ccc*-geometry was impossible.

Considering between *ttt*- and *tcc*-configurations, two azo functions in the *tcc*-configuration appeared in the *cis*-form and can compete with two different $d\pi$(Ru) orbitals during backbonding interaction while transoid geometry of azofunctions in *ttt*-configuration had compelled sharing of the same $d\pi$(Ru) orbital (Pal and Sinha, 2001). Thus, the *tcc*-configuration had a greater π-backbonding interaction than *ttt*-configuration. The greater π-backbonding interaction to azo group will increase the electron density in phenyl ring thus, the phenyl protons will appear at higher field than benzothiazole protons. From the ^{1}H NMR spectrum in Figure 36, the triplet at the most downfield position (8.00 ppm) referred to proton H10(10′) of phenyl ring followed by the proton H4(4′) (7.90 ppm) of benzothiazole ring. This may be due to the less π-backbonding interaction of azo group which corresponded to the *ttt*-configuration with *trans*-azo group. Moreover, the resonance pattern of this isomer was similar to that of *cct*-configuration which had a *trans*-azo group and the phenyl protons appeared at most downfield. Beside, the protons and carbons resonances were assigned on the basis of 1D NMR and 2D NMR spectra which showed from Figure 36 to Figure 40. Thus, it may be concluded that this isomer had *ttt*-configuration.

Table 15. ^{1}H NMR and ^{13}C NMR spectroscopic data of *ttt*-[Ru(bsazpy)$_2$Cl$_2$]

Positions	^{1}H NMR			^{13}C NMR
	δ(ppm)	J (Hz)	Number of H	δ(ppm)
10,10′	8.00 (t)	8.42	2	124.19
11,11′	7.62 (t)	7.66	1	127.05
4(4′),7(7′)	7.50 (b)	-	2	123.37
9,9′	7.25 (m)	-	2	130.29,127.65
5(5′),6(6′)	6.98 (b)	-	2	128.40
2	-	-	-	175.65
a	-	-	-	158.38
b	-	-	-	146.64
8	-	-	-	134.97

d = doublet, t = triplet, b = broad

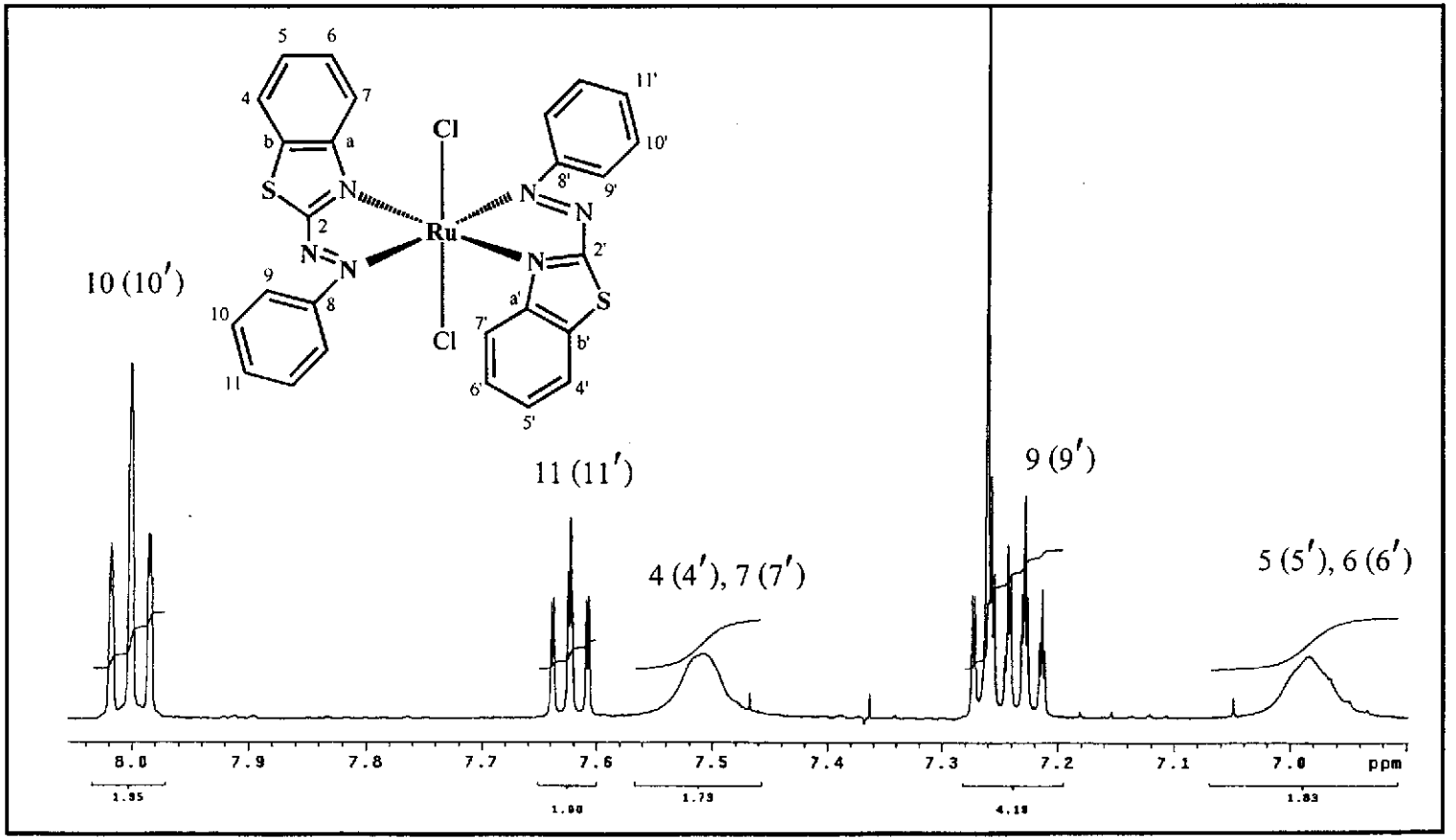

Figure 36. ^{1}H NMR spectrum of *ttt*-[Ru(bsazy)$_2$Cl$_2$] in CDCl$_3$ (500 MHz).

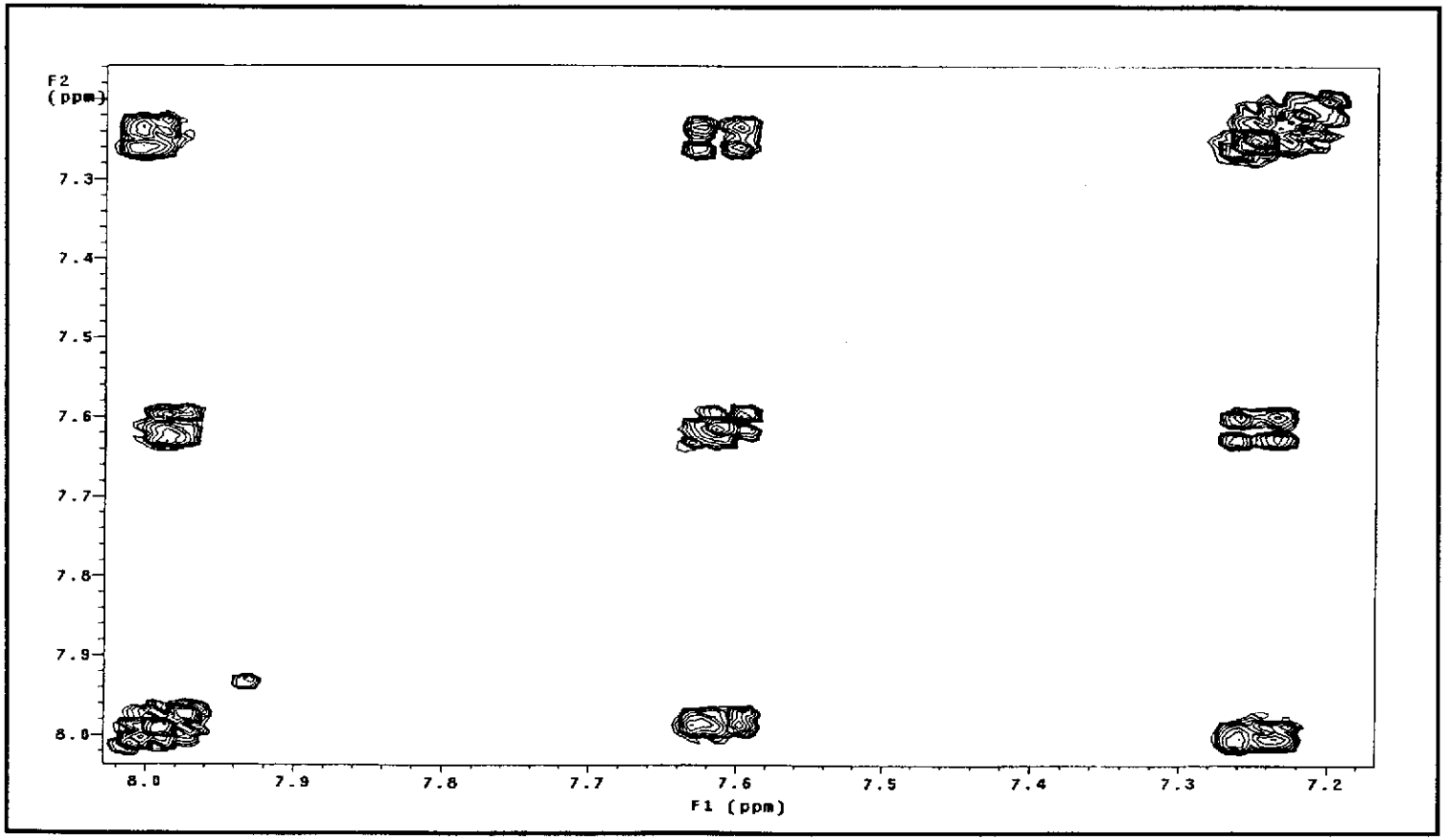

Figure 37. ^{1}H-^{1}H COSY NMR spectrum of *ttt*-$[Ru(bsazy)_2Cl_2]$ in $CDCl_3$ (500 MHz).

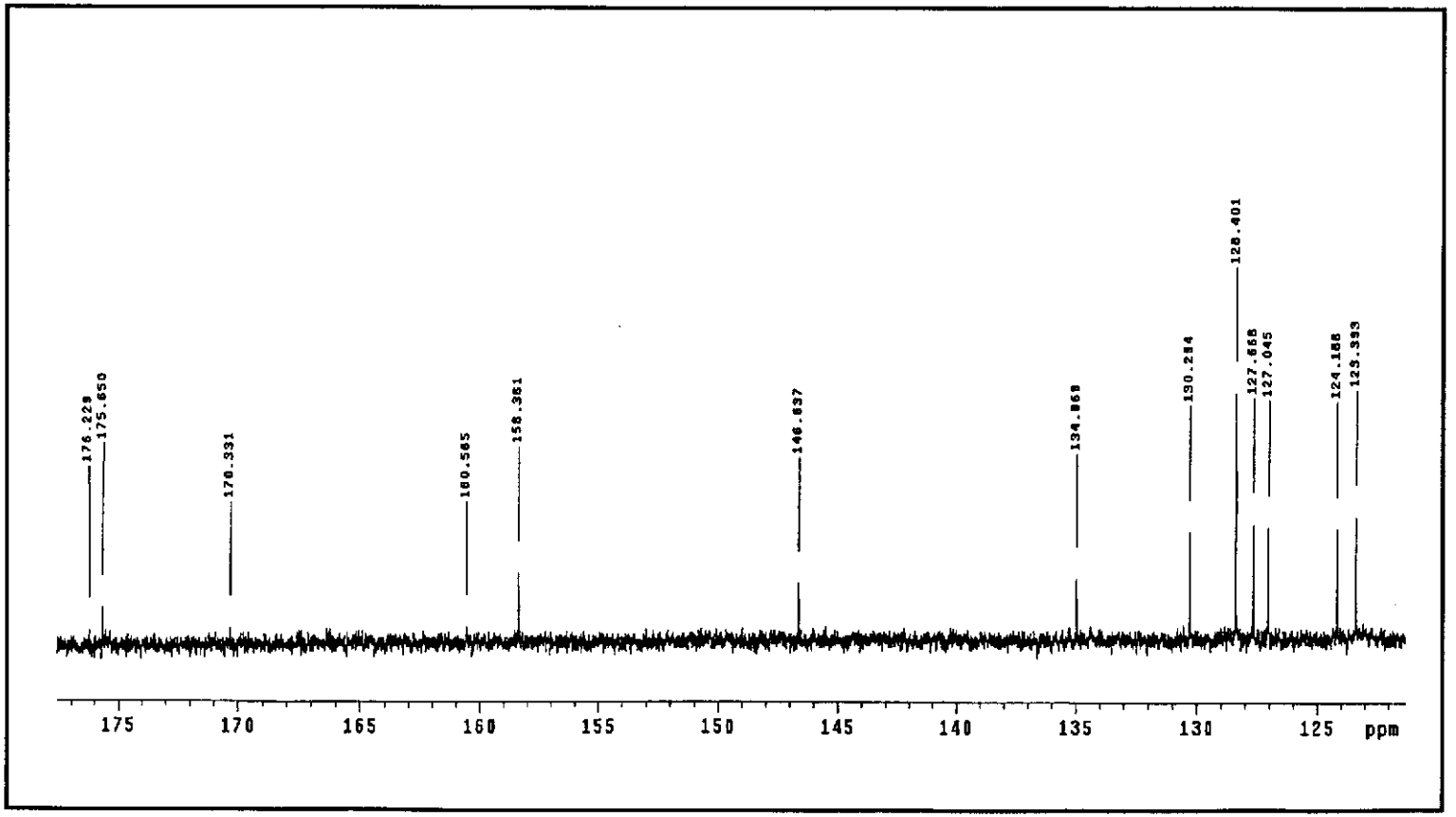

Figure 38. ^{13}C NMR spectrum of *ttt*-[Ru(bsazy)$_2$Cl$_2$] in $CDCl_3$ (500 MHz).

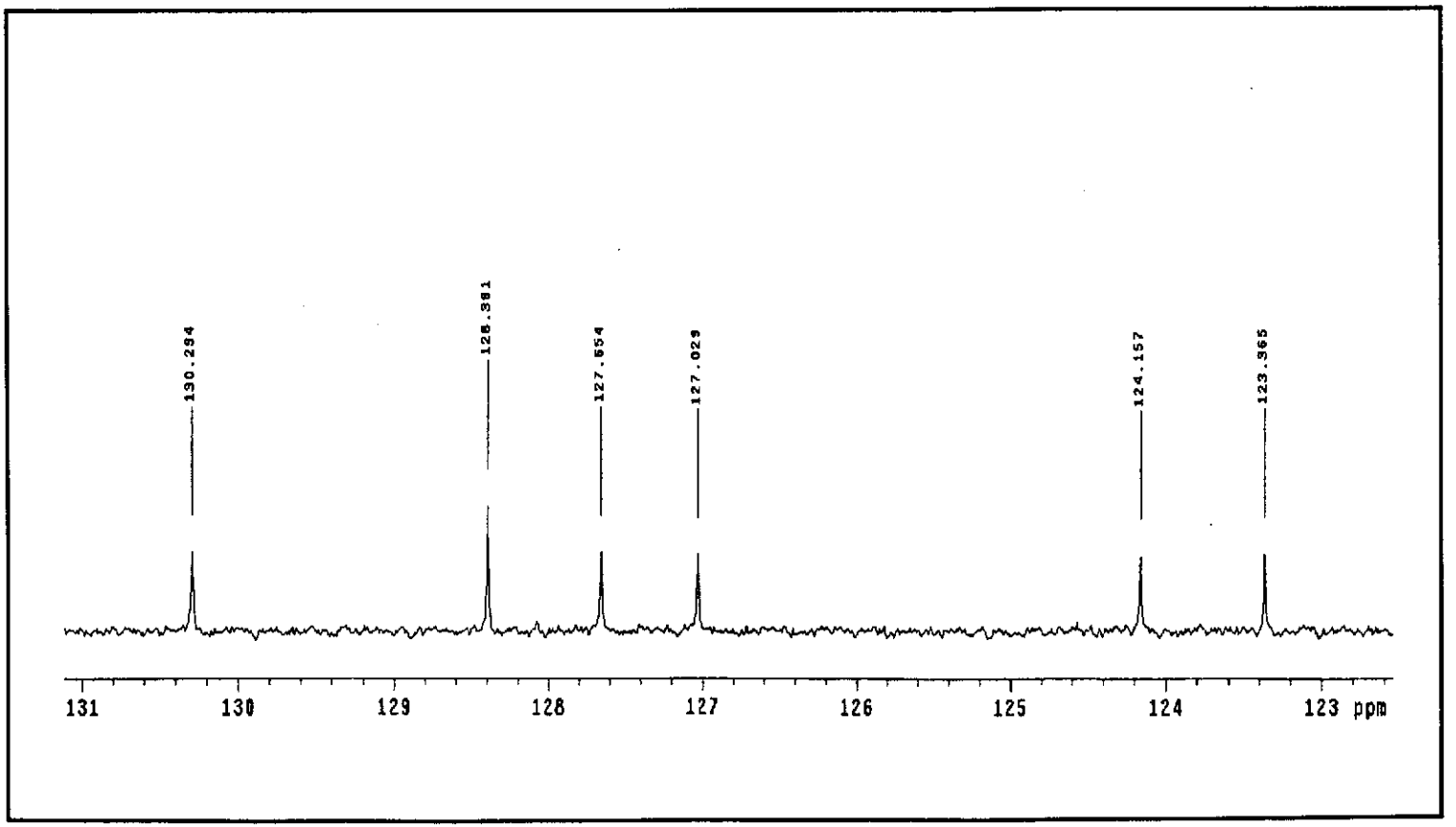

Figure 39. DEPT NMR spectrum of *ttt*-[Ru(bsazy)$_2$Cl$_2$] in $CDCl_3$ (500 MHz).

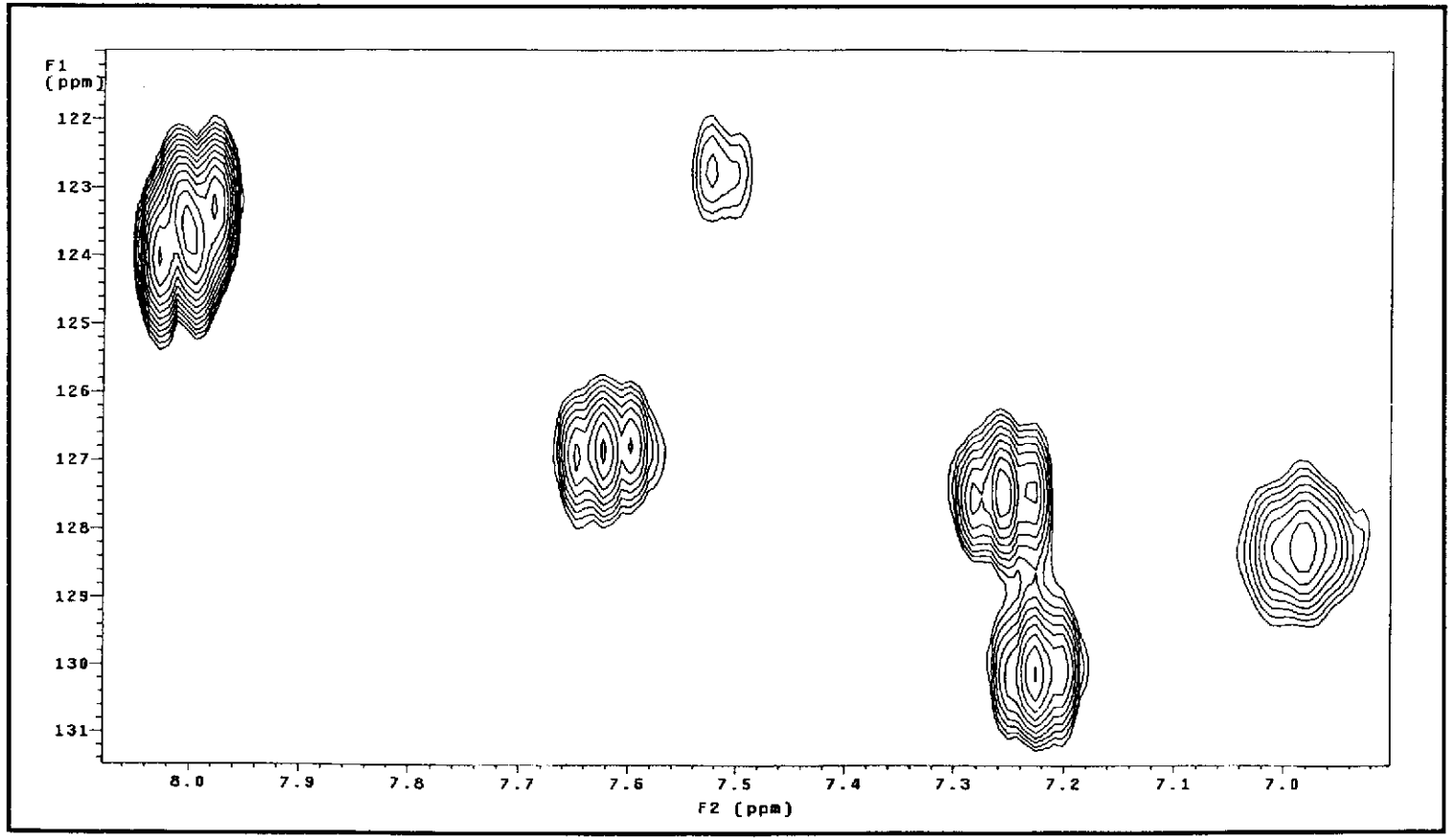

Figure 40. ^{1}H- ^{13}C HMQC NMR spectrum of *ttt*-[$Ru(bsazy)_2Cl_2$] in $CDCl_3$ (500 MHz).

3.4.6 Cyclic Voltammetry

Redox study of complexes were examined by cyclic voltammetry at a glassy carbon working electrode and the potentials were reported with reference to the ferrocene couple. The voltammograms displayed metal oxidation at the positive side and the ligand reductions at the negative side. The cyclic voltammograms in dichloromethane solution of *ctc*-, *cct*- and *ttt*-[Ru(bsazpy)$_2$Cl$_2$] complexes are shown in Figure 41 to Figure 43. The cyclic voltammetric data of the complexes are summarized in Table 16.

Table 16. Cyclic voltammetric data of the [Ru(bsazpy)$_2$Cl$_2$] complexes in 0.1 M TBAH dichloromethane at scan rate 50 mV/s (ferrocene as internal standard)

Ligands	$E_{1/2}$, V	
	Oxidation	Reduction
ctc-[Ru(bsazpy)$_2$Cl$_2$]	0.88	-0.72, -1.18[a]
cct-[Ru(bsazpy)$_2$Cl$_2$]	0.73	-0.76, -1.25[a]
ttt-[Ru(bsazpy)$_2$Cl$_2$]	0.70	-0.71, -1.21 [a]
ctc-[Ru(azpy)$_2$Cl$_2$]	0.71	-1.03, -1.55[a]

[a] Cathodic peak (Ep_c)

Oxidation range

For three [Ru(bsazpy)$_2$Cl$_2$] complexes, in the potential range 0.00 to +1.50 V at scan rate 50 mV/s reversible oxidative response was observed corresponding to the Ru(III)/Ru(II) couple which could individually transfer one electron (Eq. (3)).

$$[Ru(bsazpy)_2Cl_2]^+ + e^- \rightleftharpoons [Ru(bsazpy)_2Cl_2] \quad \ldots. (3)$$

The voltammetric patterns of the three isomers of $[Ru(bsazpy)_2Cl_2]$ complexes were very similar except the differences in Ru(III)/Ru(II) couple. The *ctc*-isomer (0.88 V) exhibited higher potentials than the *cct*-isomer (0.73 V) and the *ttt*-isomer (0.70 V) which were supported by electronic spectral data in Table 17.

Table 17. Comparison of electronic and redox properties of the $[Ru(bsazpy)_2Cl_2]$ complexes

Properties	*ctc*-isomer	*cct*-isomer	*ttt*-isomer
Ru(III)/Ru(II) , $E_{1/2}$ (V)	0.88	0.73	0.70
[a] MLCT bands, λ_{max} (nm)	618	630	645

[a] in CH_2Cl_2

The data revealed that the Ru(III)/Ru(II) couple was shifted to more positive potential and the MLCT bands were blue shifted on going from *ttt*-isomer to *ctc*-isomer. This data indicated the stability of Ru(II) in the order of *ctc*-$[Ru(bsazpy)_2Cl_2]$ > *cct*-$[Ru(bsazpy)_2Cl_2]$ > *ttt*-$[Ru(bsazpy)_2Cl_2]$.

Comparison between *ctc*-$[Ru(bsazpy)_2Cl_2]$ and *ctc*-$[Ru(azpy)_2Cl_2]$, the *ctc*-$[Ru(bsazpy)_2Cl_2]$ (0.88 V) showed the Ru(III)/Ru(II) couple at higher potentials than that of *ctc*-$[Ru(azpy)_2Cl_2]$ (0.71 V). This revealed that bsazpy ligand can stabilize the Ru(II) in the *ctc*-isomer more than azpy ligand.

Reduction range

The reductive responses were observed in the potential range 0.00 to –2.00 V. Three isomers showed one reversible couple and one cathodic peak which were referred to the electron acceptance of the azo function as Eq.(4).

$$[\text{-N=N-}] \rightleftharpoons [\text{-N-N-}]^{-} \rightleftharpoons [\text{-N-N-}]^{2-} \quad \ldots\ldots\ldots (4)$$

In three isomers, as expected, the reduction potential displayed a substitutional positive shifting from the corresponding free ligand values.

Considering the first reduction couple, the *ctc*-, *cct*- and *ttt*-$[Ru(bsazpy)_2Cl_2]$ complexes exhibited the reversible couple at –0.72, -0.76 and –0.70 V, respectively whereas the *ctc*-$[Ru(azpy)_2Cl_2]$ exhibited the reversible couple at –1.03 V. From these reduction potentials, it can be concluded that the bsazpy is easily reduced than azpy.

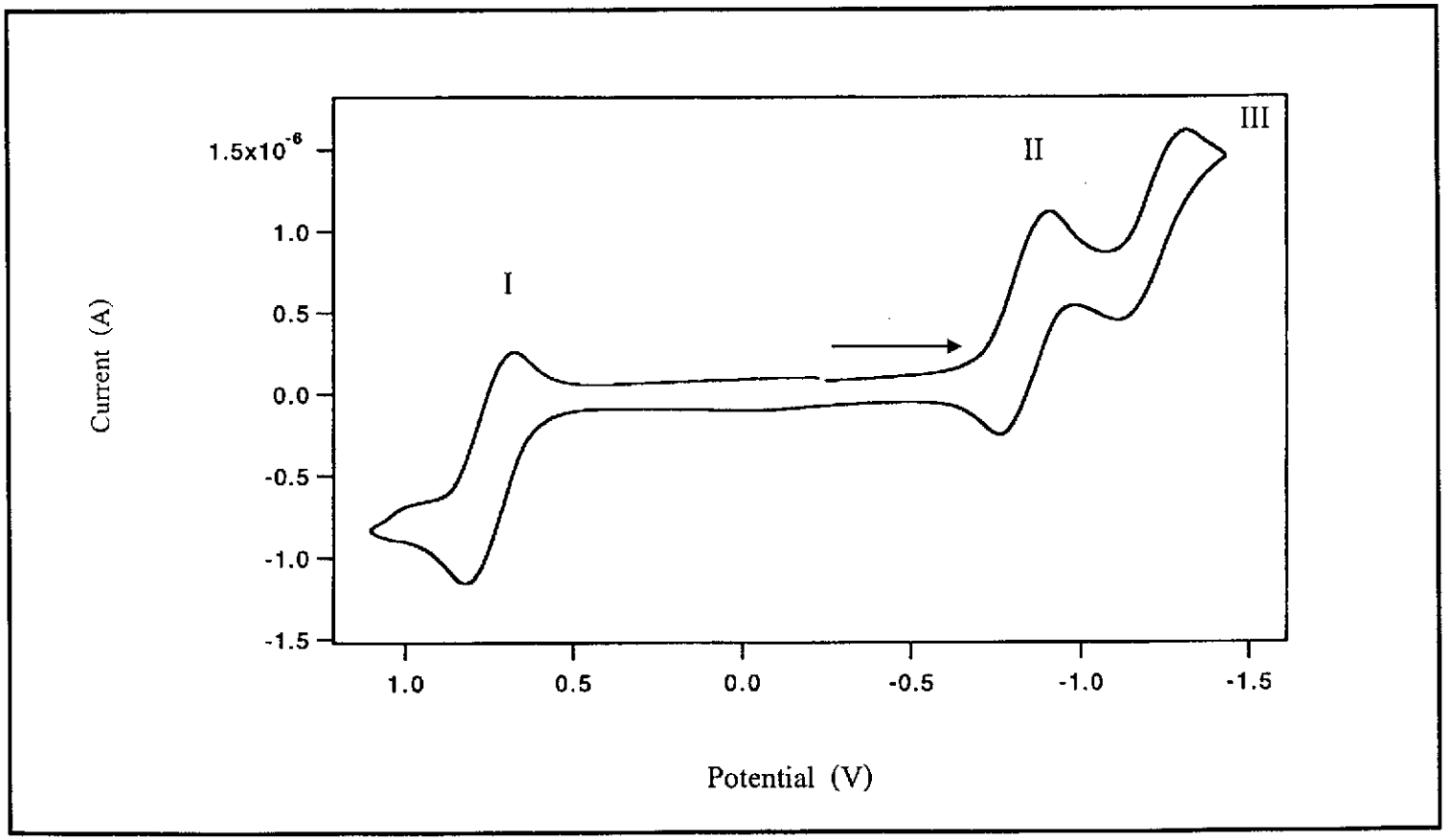

Figure 41. Cyclic voltammogram of *ctc*-[Ru(bsazpy)$_2$Cl$_2$] in 0.1 M TBAH CH_2Cl_2 at scan rate 50 mV/s.

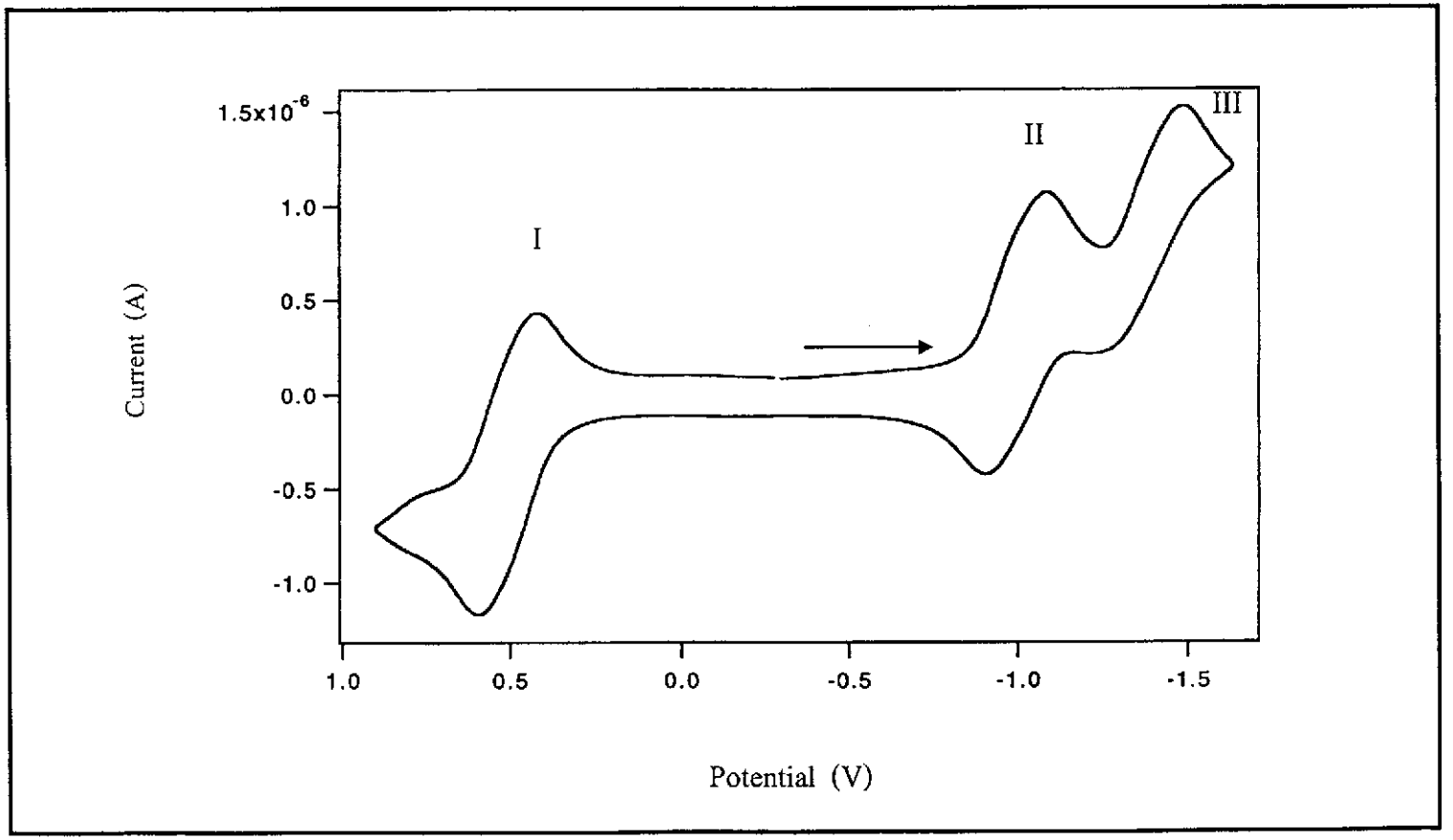

Figure 42. Cyclic voltammogram of *cct*-[Ru(bsazpy)$_2$Cl$_2$] in 0.1 M TBAH CH_2Cl_2 at scan rate 50 mV/s.

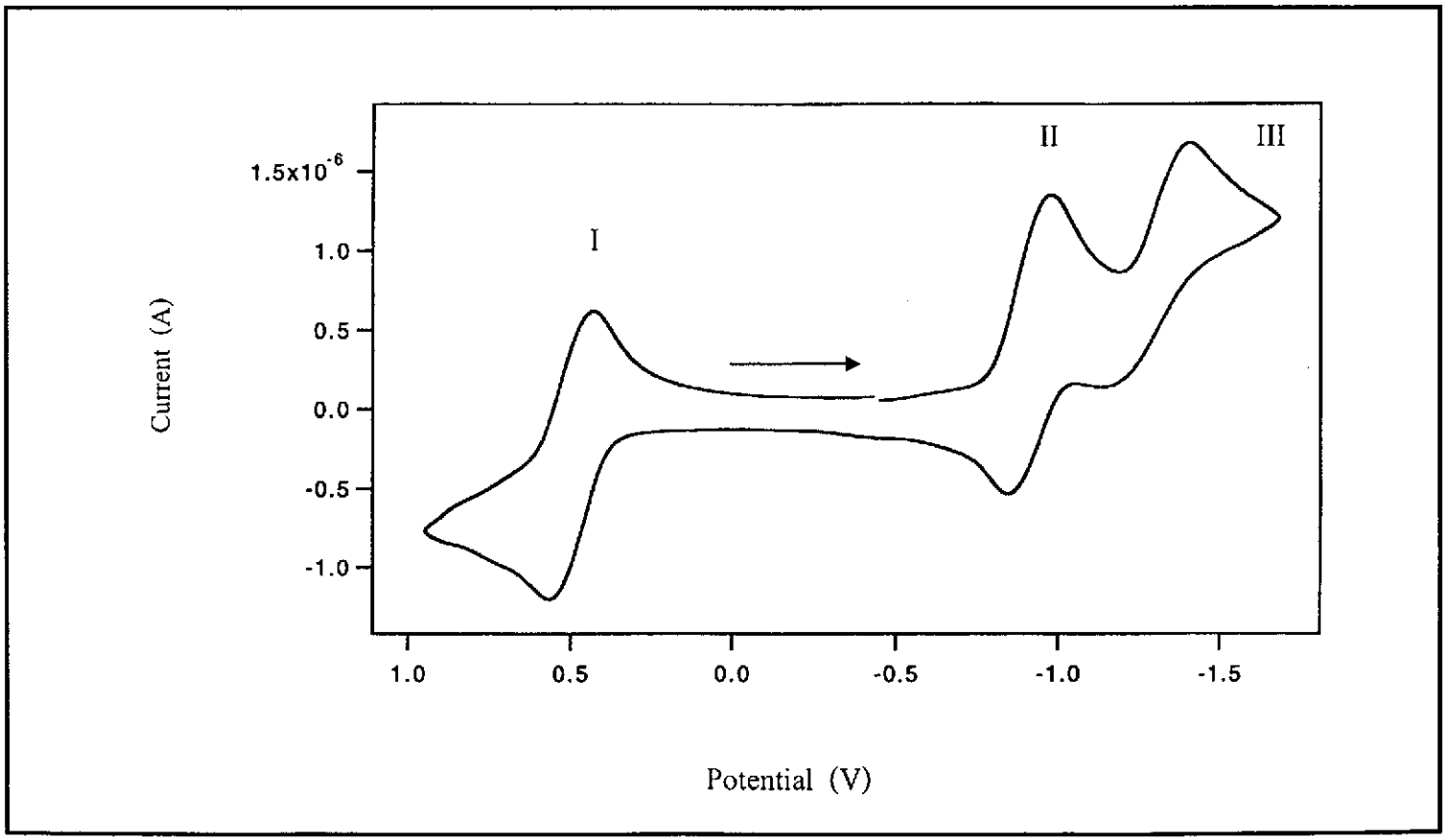

Figure 43. Cyclic voltammogram of *ttt*-[Ru(bsazpy)$_2$Cl$_2$] in 0.1 M TBAH CH_2Cl_2 at scan rate 50 mV/s.

3.4.7 X-ray Crystallography

The X-ray crystallography is an useful technique for determining the molecular structure and the configuration of molecules. The *ctc*-[Ru(bsazpy)$_2$Cl$_2$] and *cct*-[Ru(bsazpy)$_2$Cl$_2$] formed the suitable X-ray quality crystals for structure determination. The crystal structure of both complexes showed six coordination around the ruthenium center.

(a) Crystal structure of *ctc*-[Ru(bsazpy)$_2$Cl$_2$]

The X-ray quality single crystal was obtained on slow diffusion of dichloromethane solution of the complex *ctc*-[Ru(bsazpy)$_2$Cl$_2$] into acetonitrile. The crystallographic data are collected in Table 18 and the selected bond parameters are listed in Table 19.

A view of the molecule is shown in Figure 44 which showed that the coordination geometry of ruthenium(II) center is distorted octahedron. The atomic arrangement around the ruthenium center involved sequentially two *cis*-chlorides, *trans*-N(benzothiazole), N and *cis*-N(azo), N' and corresponded to *cis-trans-cis* configuration

The N(6)-Ru(1)-Cl(1) angle was 171.39(9) $^{\circ}$ and the deviation from linearity (by ~ 8.6°) was due to the acute (77.11(4) $^{\circ}$) chelate bite angle. The dihedral angle of the chelate rings, Ru-N(1)-C(7)-N(2)-N(3) and Ru-N(4)-C(20)-N(5)-N(6) was 109°. Their chelate angles were considerably deviated from ideal octahedral geometry. The most of the distortions away from octahedral positions arising out of the larger angular distortions were associated with the azo nitrogens rather than the benzothiazole nitrogens, [N(3)-Ru(1)-N(6), 103.98(10) $^{\circ}$ and N(4)-Ru(1)-N(1), 170.80(11) $^{\circ}$].

The Ru-N' [N(azo): N(3) or N(6)] bond length (average, 1.976(3) Å) was shorter than the Ru-N [N(benzothiazole): N(1) or N(4)] bond length (average, 2.029(3) Å) by 0.053 Å. The shortening may be due to greater π-backbonding, $d\pi(Ru) \rightarrow \pi^*$ (azo), offered by the azo group.

The average N-N distance was 1.30 Å which was longer than some reported values of free azo ligands (N-N ~ 1.25 Å, Ghosh *et al.*, 1984). This result corresponded to the red shift of N=N stretching frequncies from free bsazpy ligand to the complex in infrared spectrum. Moreover, the difference of two N-N bond distances were reflected in infrared spectrum which showed two N=N stretching peaks. The coordination to metal can lead to decrease in the N-N bond order due to both σ-donor and π-accepter characters of the ligand. Thus, the elongation of the N-N distance and shortening of Ru-N(azo) bond length were an indication of the existance of considerable Ru-bsazpy π-bonding with major involvement of the azo group.

Table 18. Crystallographic data for *ctc*-[Ru(bsazpy)$_2$Cl$_2$]

Empirical formula	$C_{26}\ H_{18}\ Cl_2\ N_6\ Ru\ S_2$
Formula weight	650.55
Crystal system	Monoclinic
Space group	P2(1)/n
Unit cell dimensions	a = 8.4931(7) Å $\alpha = 90^\circ$
	b = 22.0713(18) Å $\beta = 105.0160(10)^\circ$
	c = 14.3147(11) Å $\gamma = 90^\circ$
Volume	2591.7(4) Å ^{3}
Z	4
Density (calculated)	1.667 mg/m^3
Absorption coefficient	1.001 mm^{-1}
Goodness-of-fit on F^2	1.065
Final R indices [$I>2\sigma(I)$]	*R1* = 0.0161, *wR2* = 0.0394
R indices (all data)	*R1* = 0.0175, *wR2* = 0.0401

Table 19. Selected bond distances (Å) and angles (°) for *ctc*-[Ru(bsazpy)$_2$Cl$_2$]

Bond distances			
Ru(1)-N(6)	1.972(3)	N(2)-N(3)	1.297(3)
Ru(1)-N(3)	1.980(3)	N(2)-C(7)	1.360(4)
Ru(1)-N(4)	2.021(3)	N(3)-C(8)	1.431(4)
Ru(1)-N(1)	2.037(3)	N(4)-C(20)	1.331(4)
Ru(1)-Cl(2)	2.3839(9)	N(4)-C(14)	1.389(4)
Ru(1)-Cl(1)	2.3954(9)	N(5)-N(6)	1.302(3)
N(1)-C(7)	1.328(4)	N(5)-C(20)	1.355(4)
N(1)-C(1)	1.388(4)	N(6)-C(21)	1.428(4)
Bond angles			
N(6)-Ru(1)-N(3)	103.98(10)	N(4)-Ru(1)-Cl(2)	87.10(7)
N(6)-Ru(1)-N(4)	77.11(14)	N(1)-Ru(1)-Cl(2)	99.58(10)
N(3)-Ru(1)-N(4)	97.34(12)	N(6)-Ru(1)-Cl(1)	171.38(9)
N(6)-Ru(1)-N(1)	97.15(13)	N(3)-Ru(1)-Cl(1)	83.95(7)
N(3)-Ru(1)-N(1)	76.90(13)	N(4)-Ru(1)-Cl(1)	98.75(10)
N(4)-Ru(1)-N(1)	170.80(11)	N(1)-Ru(1)-Cl(1)	87.87(7)
N(6)-Ru(1)-Cl(2)	84.20(8)	Cl(2)-Ru(1)-Cl(1)	88.06(3)
N(3)-Ru(1)-Cl(2)	171.36(8)		

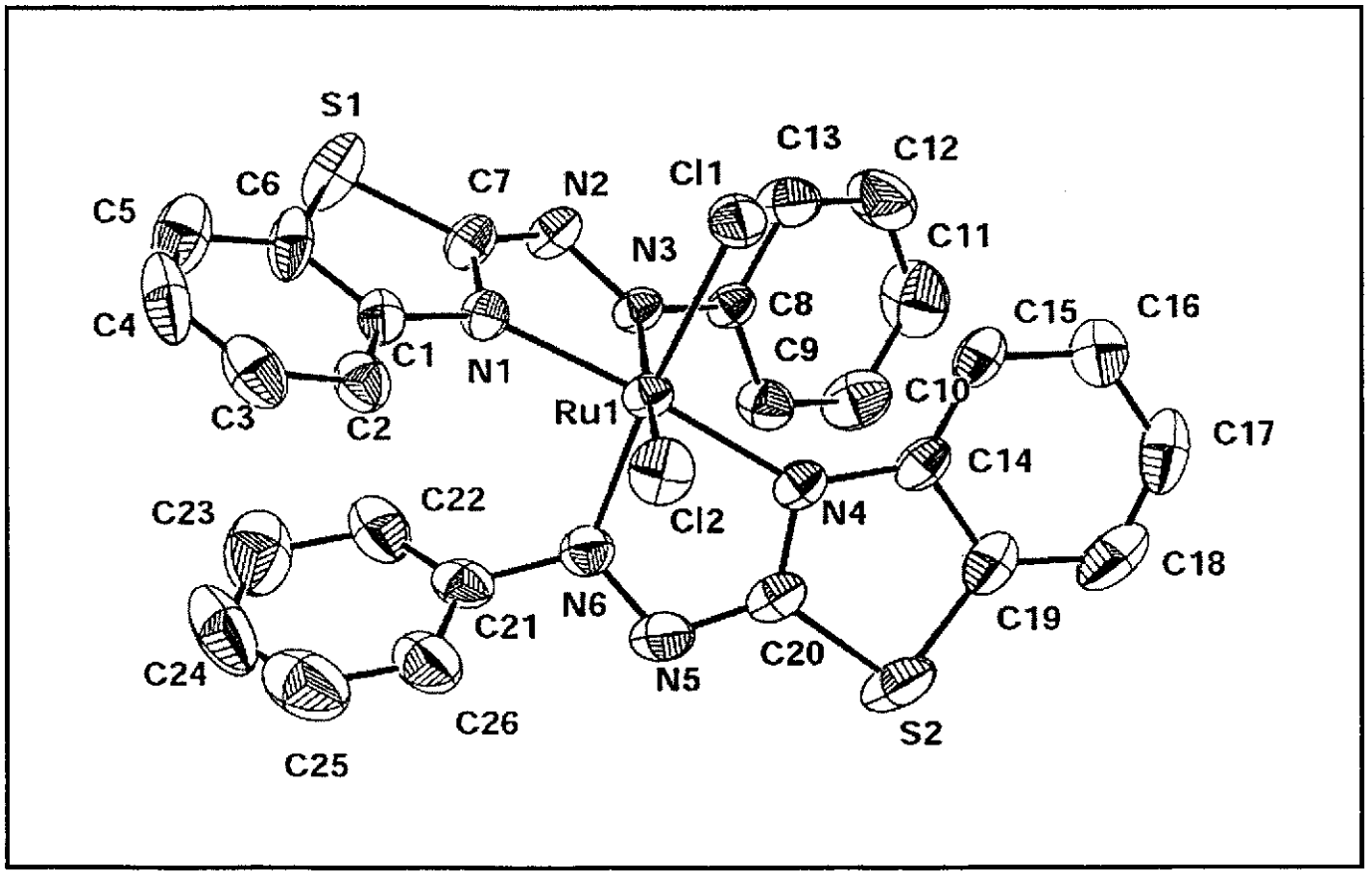

Figure 44. The crystal structure of *ctc*-[Ru(bsazpy)$_2$Cl$_2$] (H-atom omitted).

(b) Crystal structure of *cct*-[Ru(bsazpy)$_2$Cl$_2$]

The crystallographic data for the *cct*-[Ru(bsazpy)$_2$Cl$_2$] complex are collected in Table 20. Slow diffusion of a dichloromethane solution of *cct*-[Ru(bsazpy)$_2$Cl$_2$] in hexane yielded green crystal. Selected bond parameters are listed in Table 21.

Table 20. Crystallographic data for *cct*-[Ru(bsazpy)$_2$Cl$_2$]

Empirical formula	$C_{27}H_{20}Cl_4N_6RuS_2$	
Formula weight	735.48	
Crystal system	Orthorhombic	
Space group	Pbca No.61	
Unit cell dimensions	a = 17.038(3) Å	$\alpha = 90^\circ$
	b = 15.420(3) Å	$\beta = 90^\circ$
	c = 22.053(5) Å	$\gamma = 90^\circ$
Z	8	
Density (calculated)	1.686 mg/m^3	
Absorption coefficient	1.085 mm^{-1}	
Goodness-of-fit on F^2	1.097	
Final R indices [$I>2\sigma(I)$]	$R1$ = 0.0423, $wR2$ = 0.0934	
R indices (all data)	$R1$ = 0.0501, $wR2$ = 0.0973	

Table 21. Selected bond distances (Å) and angles (°) for *cct*-[Ru(bsazpy)$_2$Cl$_2$]

Bond distances			
Ru(1)-N(3)	2.017(3)	N(2)-N(3)	1.304(4)
Ru(1)-N(4)	2.023(3)	N(2)-C(7)	1.360(5)
Ru(1)-N(1)	2.024(3)	N(3)-C(8)	1.432(5)
Ru(1)-N(6)	2.070(3)	N(4)-C(20)	1.331(5)
Ru(1)-Cl(2)	2.3566(11)	N(4)-C(14)	1.393(5)
Ru(1)-Cl(1)	2.3873(11)	N(5)-N(6)	1.304(4)
N(1)-C(7)	1.331(5)	N(5)-C(20)	1.348(5)
N(1)-C(1)	1.393(5)	N(6)-C(21)	1.432(5)
Bond angles			
N(3)-Ru(1)-N(4)	100.07(12)	N(1)-Ru(1)-Cl(2)	170.29(9)
N(3)-Ru(1)-N(1)	76.30(12)	N(6)-Ru(1)-Cl(2)	82.60(9)
N(4)-Ru(1)-N(1)	95.33(12)	N(3)-Ru(1)-Cl(1)	85.30(9)
N(3)-Ru(1)-N(6)	175.62(12)	N(4)-Ru(1)-Cl(1)	174.63(9)
N(4)-Ru(1)-N(6)	76.09(13)	N(1)-Ru(1)-Cl(1)	85.89(9)
N(1)-Ru(1)-N(6)	105.97(12)	N(6)-Ru(1)-Cl(1)	98.54(9)
N(3)-Ru(1)-Cl(2)	95.47(9)	Cl(2)-Ru(1)-Cl(1)	88.33(4)
N(4)-Ru(1)-Cl(2)	91.15(9)		

A view of the molecular unit of *cct*-[Ru(bsazpy)$_2$Cl$_2$] is shown in Figure 45 which showed the distorted octahedron structure. The atomic arrangement around the ruthenium center involved sequentially two *cis*-chlorides, *cis*-N(benzothiazole), N and *trans*-N(azo), N' and corresponded to *cis-cis-trans* configuration.

The *trans* angles around the ruthenium center in the planes ranged from 170.29(9)° to 175.62(12)°, indicating distortion from rectilinear geometry. The dihedral angle of the chelate rings, Ru-N(1)-C(7)-N(2)-N(3) and Ru-N(4)-C(20)-N(5)-N(6) was 84° . Their chelate angles were considerably deviated from ideal octahedral geometry. It was interesting that most of the distortions away from octahedral positions arising out of the larger angular distortions were associated with the benzothiazole nitrogens rather than the azo nitrogens, [N(4)-Ru(1)-N(1), 95.33(12)° and N(3)-Ru(1)-N(6), 175.62(12)°].

The Ru-N' [N(azo): N(3)] bond length (2.017(3) Å) was shorter than the Ru-N [N(benzothiazole): N(1) or N(4)] bond length (average, 2.024(3) Å) by 0.053 Å. The shortening may be due to greater π-backbonding, $d\pi(Ru) \longrightarrow \pi^*$ (azo), offered by the azo group. The Ru-N' [N(azo): N(6)] (2.070(3) Å) bond distance was longer than Ru-N' [N(azo): N(6)]. This data revealed the less π-acceptor ability of the former azo group which may be due to the *trans*-configuration of two azo groups.

Similarly, average N-N distance was 1.30 Å which was longer than some reported values of free azo ligands (N-N ~ 1.25 Å, Ghosh *et al.*, 1984). This result corresponded to the red shift of N=N stretching frequncies from free bsazpy ligand to the complex in infrared spectrum. The coordination can lead to decrease in the N-N bond order due to both σ-donor and π-accepter characters of the ligand, the later character had a more pronounced effect and was possibly the reason for elongation.

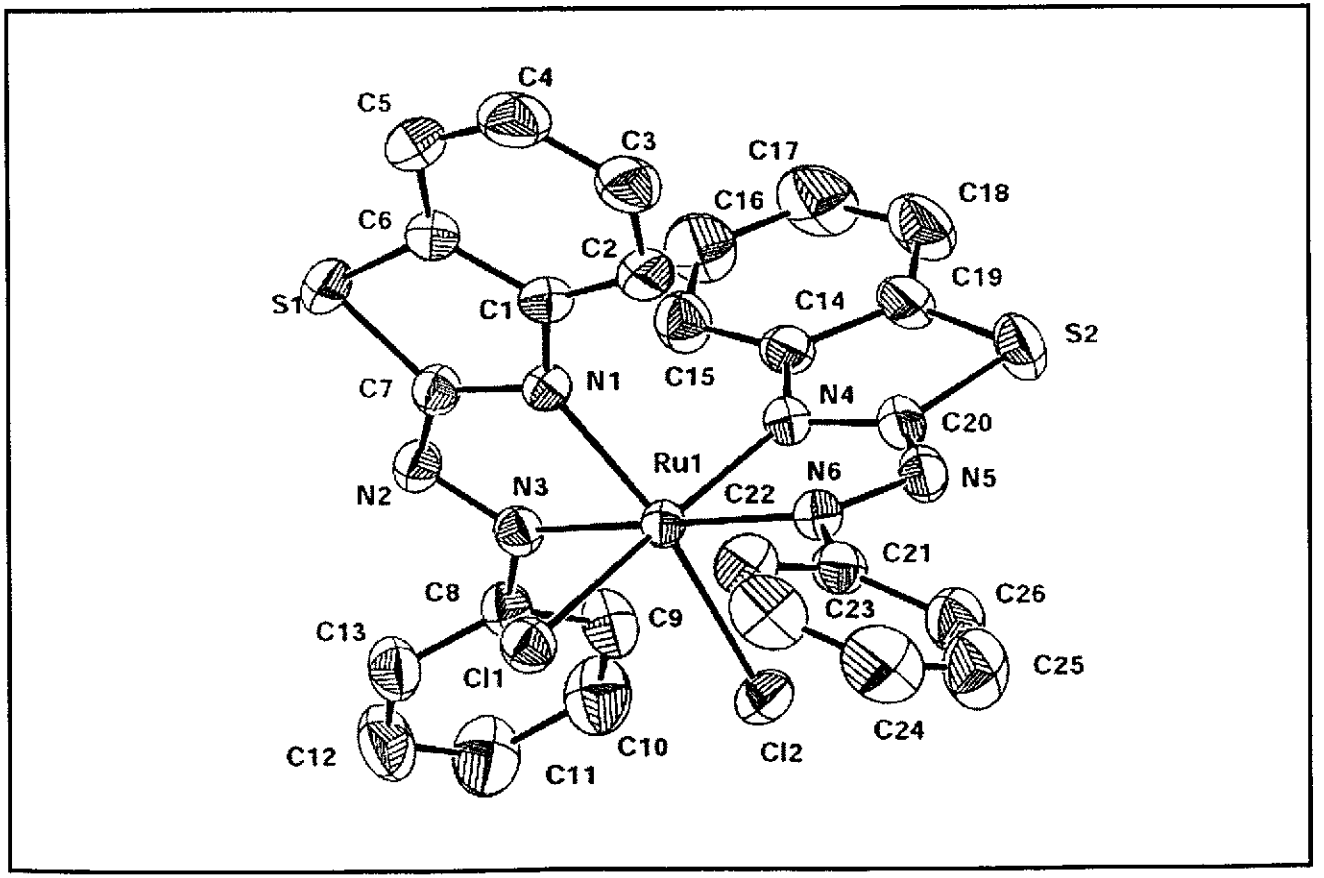

Figure 45. The crystal structure of *cct*-[Ru(bsazpy)$_2$Cl$_2$] (H-atom omitted).